

AD-A204 025

DTIC FILE COPY

4

RADC-TR-88-189  
Final Technical Report  
September 1988



# THE VANE-LOADED LADDER SLOW-WAVE CIRCUIT

University of Utah

Robert A. Koshgarian

APPROVED FOR PUBLIC RELEASE; DISTRIBUTION UNLIMITED.

DTIC  
ELECTE  
S 14 FEB 1989 D  
E

ROME AIR DEVELOPMENT CENTER  
Air Force Systems Command  
Griffiss Air Force Base, NY 13441-5700

89 2 13 269

This report has been reviewed by the RADC Public Affairs Division (PA) and is releasable to the National Technical Information Service (NTIS). At NTIS it will be releasable to the general public, including foreign nations.

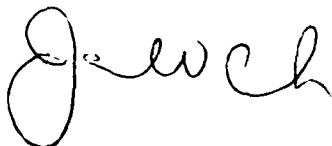
RADC-TR-88-189 has been reviewed and is approved for publication.

APPROVED:



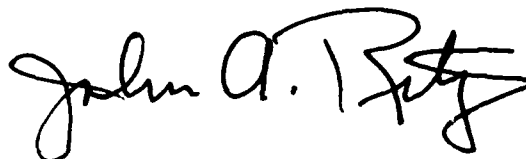
ANDREW E. CHROSTOWSKI, CAPT, USAF  
Project Engineer

APPROVED:



JAMES W. CUSACK  
Acting Director of Surveillance

FOR THE COMMANDER:



JOHN A. RITZ  
Directorate of Plans & Programs

If your address has changed or if you wish to be removed from the RADC mailing list, or if the addressee is no longer employed by your organization, please notify RADC (OCTP) Griffiss AFB NY 13441-5700. This will assist us in maintaining a current mailing list.

Do not return copies of this report unless contractual obligations or notice on a specific document requires that it be returned.

11/12/88

REPORT DOCUMENTATION PAGE				Form Approved OMB No. 0704-0188	
1a. REPORT SECURITY CLASSIFICATION UNCLASSIFIED			1b. RESTRICTIVE MARKINGS N/A		
2a. SECURITY CLASSIFICATION AUTHORITY N/A			3. DISTRIBUTION / AVAILABILITY OF REPORT Approved for public release; distribution unlimited.		
2b. DECLASSIFICATION / DOWNGRADING SCHEDULE N/A					
4. PERFORMING ORGANIZATION REPORT NUMBER(S) UTEC MD 87-087			5. MONITORING ORGANIZATION REPORT NUMBER(S) RADC-TR-88-189		
6a. NAME OF PERFORMING ORGANIZATION University of Utah		6b. OFFICE SYMBOL (if applicable)	7a. NAME OF MONITORING ORGANIZATION Rome Air Development Center (OCTP)		
6c. ADDRESS (City, State, and ZIP Code) Microwave Device & Physical Electronics Lab Department of Electrical Engineering Salt Lake City UT 84112			7b. ADDRESS (City, State, and ZIP Code) Griffiss AFB NY 13441-5700		
8a. NAME OF FUNDING / SPONSORING ORGANIZATION AFOSR		8b. OFFICE SYMBOL (if applicable) NE	9. PROCUREMENT INSTRUMENT IDENTIFICATION NUMBER F30602-84-C-0153		
8c. ADDRESS (City, State, and ZIP Code) Bolling AFB Wash DC 20332			10. SOURCE OF FUNDING NUMBERS		
			PROGRAM ELEMENT NO. 61102F	PROJECT NO. 2305	TASK NO. J9
					WORK UNIT ACCESSION NO. 17
11. TITLE (Include Security Classification) THE VANE-LOADED LADDER SLOW-WAVE CIRCUIT					
12. PERSONAL AUTHOR(S) Robert A. Koshgarian					
13a. TYPE OF REPORT Final		13b. TIME COVERED FROM Sep 84 to Sep 87		14. DATE OF REPORT (Year, Month, Day) September 1988	
15. PAGE COUNT 84					
16. SUPPLEMENTARY NOTATION Research was accomplished in conjunction with Air Force Thermionics Engineering Research Program (AFTER) AFTER-26. Robert A. Koshgarian was an AFTER student from the Raytheon Company. This report was submitted in partial fulfillment (See Reverse)					
17. COSATI CODES			18. SUBJECT TERMS (Continue on reverse if necessary and identify by block number)		
FIELD	GROUP	SUB-GROUP	Ladder Circuit, Crossed Field Amplifiers (CFA),		
09	01		Vane Loaded, Traveling Wave Tubes. <i>mgm</i>		
			Slow Wave		
19. ABSTRACT (Continue on reverse if necessary and identify by block number) This paper investigates the vane loaded ladder slow wave circuit. This circuit, derived from the interdigital line, is examined as a possible alternative to circuits currently used in crossed field amplifiers (CFA's). Its configuration is designed to possess wideband dispersion and to allow access to the fundamental forward-wave space harmonic through altered electric field distributions.  The analytical results show that the circuit possesses intrinsic shortcomings which prevent full realization of the desired features. While it does preserve the wideband dispersion of the interdigital line, it also introduces some undesirable characteristics. Furthermore, the new electric field distributions contribute to the desired impedance behavior only under limited circumstances. In general, the impedance characteristics which inhibit the interdigital line as a forward-wave circuit are present in the new circuit to the same degree. It is concluded that typical CFA circuits, such as the stub-support meander line, are more advantageous.					
20. DISTRIBUTION / AVAILABILITY OF ABSTRACT <input checked="" type="checkbox"/> UNCLASSIFIED/UNLIMITED <input type="checkbox"/> SAME AS RPT. <input type="checkbox"/> DTIC USERS			21. ABSTRACT SECURITY CLASSIFICATION UNCLASSIFIED		
22a. NAME OF RESPONSIBLE INDIVIDUAL Andrew E. Chrostowski, Capt, USAF			22b. TELEPHONE (Include Area Code) (315) 330-4381		22c. OFFICE SYMBOL RADC (OCTP)

UNCLASSIFIED

16. SUPPLEMENTARY NOTATION (Continued).

of the requirements for the degree of Electrical Engineering.

UNCLASSIFIED

# ABSTRACT

This paper investigates the vane-loaded ladder slow-wave circuit. This circuit, derived from the interdigital line, is examined as a possible alternative to circuits currently used in crossed-field amplifiers (CFA's). Its configuration is designed to possess wideband dispersion and to allow access to the fundamental forward-wave space harmonic through altered electric field distributions.

The analytical results show that the circuit possesses intrinsic shortcomings which prevent full realization of the desired features. While it does preserve the wideband dispersion of the interdigital line, it also introduces some undesirable characteristics. Furthermore, the new electric field distributions contribute to the desired impedance behavior only under limited circumstances. In general, the impedance characteristics which inhibit the interdigital line as a forward-wave circuit are present in the new circuit to the same degree. It is concluded that typical CFA circuits, such as the stub-supported meander line, are more advantageous.



Accession For	
NTIS GRA&I	<input checked="" type="checkbox"/>
DTIC TAB	<input type="checkbox"/>
Unannounced	<input type="checkbox"/>
Justification	
By _____	
Distribution/	
Availability Codes	
Dist	Avail and/or Special
A-1	

## ACKNOWLEDGMENTS

I am truly grateful to Dr. Norman Dionne for his endless patience in helping me to understand the intricacies of the theory and for his genuine concern and guidance. Without his help, this work would not have been possible. I would like to thank Dr. Alan Palevsky for many helpful discussions and for his contributions to the development of the computer program used to model the circuits. I would also like to thank the Raytheon Company, the University of Utah, and the US Air Force for allowing me to participate in the AFTER program.

Most of all, I am grateful to my wife Monica for her patience and support.

# TABLE OF CONTENTS

	<u>Page</u>
I. INTRODUCTION . . . . .	1
II. REVIEW OF THE INTERDIGITAL SLOW-WAVE CIRCUIT . . . . .	3
A. Circuit Illustration and Description . . . . .	3
B. Dispersion Characteristic . . . . .	3
C. Beam Coupling Impedance . . . . .	14
1. Group Velocity $v_g$ . . . . .	15
2. Stored Energy Per Pitch $W_s$ . . . . .	16
3. Electric Field Distribution $E_n E_n^*$ . . . . .	17
4. Final Expressions for Beam Coupling Impedance . .	21
III. ANALYSIS OF THE VANE-LOADED LADDER SLOW-WAVE CIRCUIT . . .	29
A. Circuit Illustration and Description . . . . .	29
B. Dispersion Characteristic . . . . .	31
C. Beam Coupling Impedance . . . . .	43
1. Group Velocity $v_g$ . . . . .	43
2. Stored Energy Per Pitch . . . . .	44
3. Electric Field Distribution $E_n E_n^*$ . . . . .	44
4. Final Expressions for Beam Coupling Impedance . .	45
IV. DISCUSSION . . . . .	57
V. CONCLUSION . . . . .	68
REFERENCES . . . . .	70
APPENDIX A. LIST OF SYMBOLS . . . . .	71

# LIST OF ILLUSTRATIONS

<u>Figure</u>		<u>Page</u>
1	Interdigital slow-wave circuit . . . . .	4
2	Admittance function $Y(\theta)$ . . . . .	8
3	First passband of the interdigital slow-wave circuit . . .	13
4a	Beam coupling impedance for the primary interdigital space harmonics . . . . .	23
4b	$K^1$ for the primary interdigital space harmonics . . . . .	24
4c	$K^2$ for the primary interdigital space harmonics . . . . .	25
5a	Beam coupling impedance for the secondary interdigital space harmonics . . . . .	26
5b	$K^1$ for the secondary interdigital space harmonics . . . .	27
5c	$K^2$ for the secondary interdigital space harmonics . . . .	28
6	Vane-loaded ladder slow-wave circuit . . . . .	30
7	Vane-loaded ladder as a consolidation of two interdigital slow-wave circuits . . . . .	32
8	Vane-loaded ladder bisected into two equal regions . . . .	34
9	First passband of the vane-loaded ladder slow-wave circuit . . . . .	42
10a	Beam coupling impedance for the primary vane-loaded ladder space harmonics ( $\phi_b = \phi_o, 2\phi_o$ ) . . . . .	47
10b	Beam coupling impedance for the primary vane-loaded ladder space harmonics ( $\phi_b = \phi_o/2$ ) . . . . .	48
10c	Beam coupling impedance for the primary vane-loaded ladder space harmonics ( $\phi_b = \phi_o/4$ ) . . . . .	49
10d	$K^1$ for the primary vane-loaded ladder space harmonics ( $\phi_b = 2\phi_o, \phi_o, \phi_o/2, \phi_o/4$ ) . . . . .	50
10e	$K^2$ for the primary vane-loaded ladder space harmonics . .	51
11a	Beam coupling impedance for the secondary vane-loaded ladder space harmonics ( $\phi_b = \phi_o, 2\phi_o$ ) . . . . .	52



<u>Figure</u>		<u>Page</u>
11b	Beam coupling impedance for the secondary vane-loaded ladder space harmonics ( $\phi_b = \phi_o/2$ ) . . . . .	53
11c	Beam coupling impedance for the secondary vane-loaded ladder space harmonics ( $\phi_b = \phi_o/4$ ) . . . . .	54
11d	$K^1$ for the secondary vane-loaded ladder space harmonics ( $\phi_b = 2\phi_o, \phi_o, \phi_o/2, \phi_o/4$ ) . . . . .	55
11e	$K^2$ for the secondary vane-loaded ladder space harmonics . . . . .	56
12	Phase velocities for the primary and secondary forward-wave components (both circuits) . . . . .	59
13a	Electric field modulation for the primary vane-loaded ladder space harmonics (low end of band) . . . . .	63
13b	Electric field modulation for the primary vane-loaded ladder space harmonics (mid-band) . . . . .	64
13c	Electric field modulation for the primary vane-loaded ladder space harmonics (high end of band) . . . . .	65

## I. INTRODUCTION

The interdigital slow-wave circuit was first analyzed by Fletcher<sup>1</sup> in 1952. It has since been used extensively for microwave generation, particularly in M-type backward-wave oscillators (M-BWO's). It is well suited for use in M-BWO's because of the large impedance bandwidth of the primary backward-wave space harmonic. In a crossed-field, forward-wave amplifier, however, the interdigital line would be less desirable. Because of the disparity in the beam coupling impedances for the primary forward- and backward-wave space harmonics, the gain of the amplifier would be less than a comparable backward-wave amplifier and preventing oscillation would be difficult. The problem of unwanted oscillation can be eased by interacting with other forward-wave space harmonics, but this reduces the beam coupling impedance and also entails a reduction in bandwidth. As a result, in M-type amplifiers, the interdigital line is disregarded in favor of circuits such as the stub-supported meander line, for which the impedance behavior, among other factors, is more favorable. The price paid for this is the narrow-band dispersion of the stub-supported meander line's fundamental forward-wave space harmonic.

This report investigates a slow-wave circuit which may serve as an alternative to circuits currently used in crossed-field amplifiers (CFA's). It is called the vane-loaded ladder. This circuit was originally conceived as a consolidation of two adjacent interdigital lines. Such a configuration is designed to preserve the wideband dispersion of the interdigital line while increasing its potential as a forward-wave

circuit by altering the impedance behavior of the primary space harmonics.

Since the analysis of the new circuit relies heavily on an understanding of the interdigital line, the report begins in Chapter II with a review of the interdigital line. The report then proceeds to Chapter III, where the analysis of the vane-loaded ladder is given. The procession of this chapter closely parallels that of Chapter II. In Chapter IV, the results of the previous chapters are discussed and the new circuit is evaluated. Conclusions are then presented in Chapter V.

## II. REVIEW OF THE INTERDIGITAL SLOW-WAVE CIRCUIT

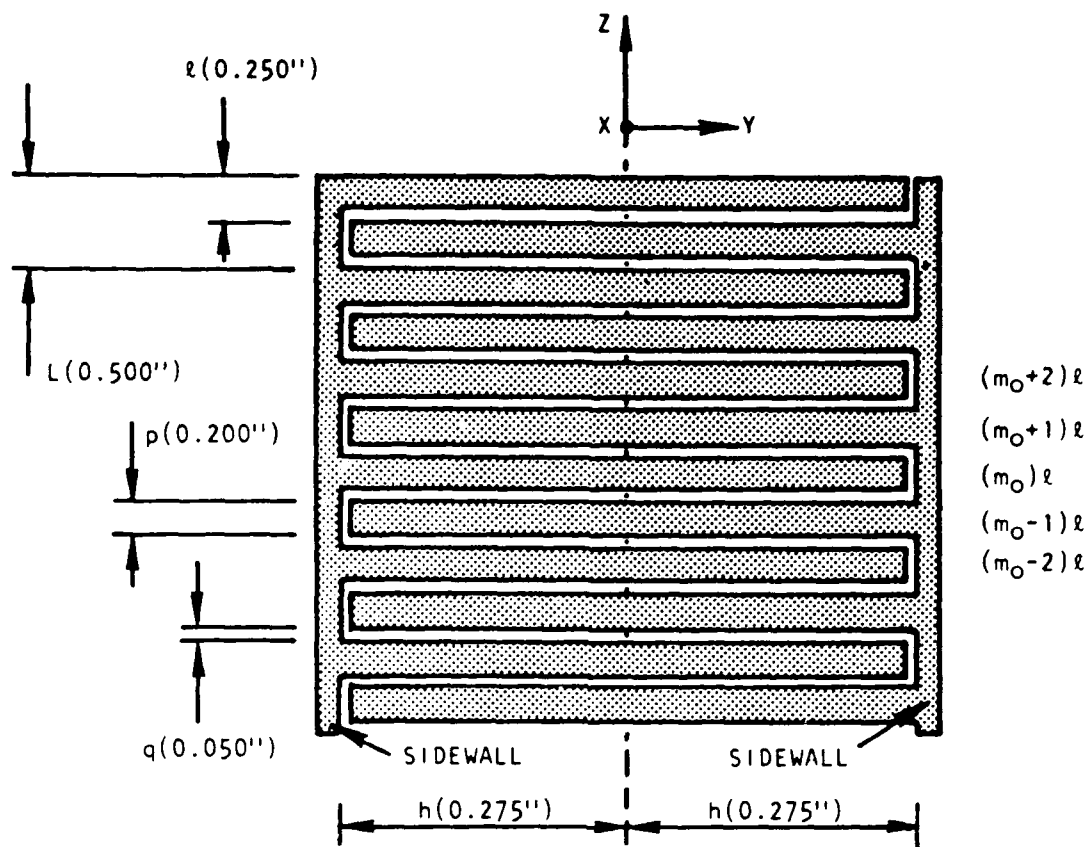
Before examining the vane-loaded ladder, it is useful to review the analysis of the interdigital line as first presented by Fletcher.<sup>1</sup> This serves two purposes. First, it provides an introduction to the analysis by way of an easy-to-follow example. Second, it exposes the deficiencies of the interdigital line which provided the motivation for investigating a new circuit.

### A. Circuit Illustration and Description

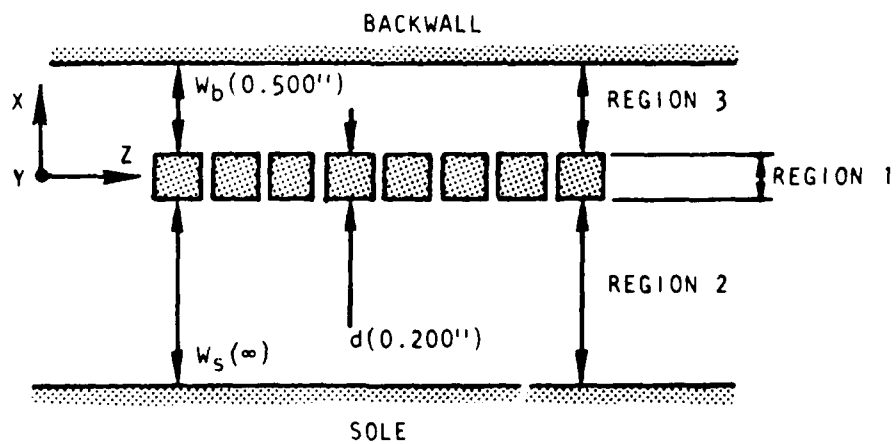
The interdigital line is illustrated in Fig. 1. It is a planar circuit composed of two sets of interlaced, straight fingers of length  $2h$  which originate at their respective sidewalls and extend almost the entire width of the circuit to the opposite sidewall. The pitch,  $\ell$ , is the center-to-center distance between adjacent fingers of opposite type, and the period,  $L = 2\ell$ , is the similarly defined distance between adjacent fingers of the same type. The circuit may also be loaded by a backwall and/or sole as shown. These are both attached to the sidewalls and are considered to be at ground potential (see below).

### B. Dispersion Characteristic

As Ash and Studd<sup>3</sup> point out, Fletcher's method of analysis<sup>1</sup> employs two distinct approximations. First, it is assumed that the fields on the circuit can be approximated by TEM waves which travel between the fingers in the direction of the fingers ( $\pm y$  direction in Fig. 1). These waves travel with the free-space speed of light,  $c$ , and wave number,  $k = \omega/c$ . In the absence of an electric field component in the direction



(a) Top view.



(b) Side view.

Fig. 1. Interdigital slow-wave circuit.

of the fingers,  $\text{curl } \vec{E}$  is zero in the plane transverse to the fingers, and therefore a voltage can be defined in that plane which satisfies the two-dimensional Laplace equation.

$$\frac{\delta^2 V}{\delta x^2} + \frac{\delta^2 V}{\delta z^2} = 0 \quad (1)$$

With the introduction of an impedance function, the corresponding current can also be expressed. The presence of such voltage and current allows the second approximation to be made, namely that Kirchoff's equations are satisfied on the circuit rather than Maxwell's equations. To satisfy Maxwell's equations on the periodic circuit, electric and magnetic fields composed of infinite sums of space harmonics would be required. The phase shift per pitch for the  $n$ th space harmonic,  $\theta_n$ , would then be

$$\theta_n = \beta_n l = \frac{\beta_n L}{2} = \theta + n\pi \quad (2)$$

where

$$\beta_n = \beta_0 + 2\pi n/L = \text{propagation constant for the } n\text{th space harmonic} \quad (3)$$

Using Kirchoff's equations, however, voltage and current composed of just two space harmonics are sufficient to satisfy the boundary conditions (because of the form of the solution to the two-dimensional Laplace equation, space harmonics whose propagation constants differ by

integral multiples of  $2\pi$  are indistinguishable from one another). Thus, the voltage at a given position on the  $m$ th finger is given by

$$\begin{aligned} V^m(\phi) &= \left[ A e^{-jm\theta} + B e^{-jm(\theta+\pi)} \right] e^{-j\phi} \\ &= \left[ A_1 \sin \phi + A_2 \cos \phi \right] e^{-jm\theta} + \left[ A_3 \sin \phi + A_4 \cos \phi \right] e^{-jm(\theta+\pi)} \end{aligned} \quad (4)$$

where

$$\phi = \omega x / c \quad (5)$$

The latter form of the voltage reveals an important aspect of the analysis, namely the use of symmetric (cosine, which is symmetric around the origin) and antisymmetric (sine, which is antisymmetric about the origin) standing waves to satisfy the boundary conditions.

In order to express the current associated with a given voltage, Fletcher<sup>1</sup> introduced the admittance function  $Y(\theta)$ . This function is defined as the ratio of the current to the voltage at any point on the circuit for a given value of  $\theta$ . Walling,<sup>2</sup> who corrected Fletcher's original expression,<sup>1</sup> gives this admittance function as

$$Y(\theta) = Y_0 \left\{ (u_d/q) \sin(\theta/2) + 2(1 - \alpha) \sin(\theta/2) [S(w_b, \alpha) + S(w_s, \alpha)] \right\} \quad (6)$$

where

$$Y_0 = \sqrt{\epsilon_0 / \mu_0} = \text{admittance of free space} \quad (7)$$

$$\alpha = q/p \quad (8)$$

$$\sigma = (\theta/2) + n\pi \quad (9)$$

and

$$S(w, \alpha) = \sum (-1)^n \coth [2w\sigma/1] \frac{\sin [(1 - \alpha)\sigma]}{[(1 - \alpha)\sigma]} \frac{\sin [\alpha\sigma]}{[\alpha\sigma]} \quad (10)$$

The summation in Eq. 10 is from  $n = -\infty$  to  $n = +\infty$ . This admittance function, which is plotted in Fig. 2, has several important features which merit special attention. First, it is independent of position. The admittance depends only on  $\theta$ , the circuit dimensions, and the back-wall and sole spacings  $w_b$  and  $w_s$ , respectively. Because it is a function of  $\theta$ , it is different for each of the space harmonics which comprise the voltage. Second, the admittance function contains all information regarding the behavior of the fields in the direction perpendicular to the plane of the circuit (more precisely, this information is wholly contained in the function  $S$ ). This is beneficial because it reduces the analysis to a two-dimensional one. Finally, the function  $S$  is composed (ideally) of an infinite sum of space harmonics, thereby providing the link between the two-harmonic approximation and the infinite, exact solution.

The general expression for the current is

$$I(\phi) = jY(\theta) \frac{\delta V(\phi)}{\sigma \phi} \quad (11)$$

which when applied to each space harmonic of the voltage gives



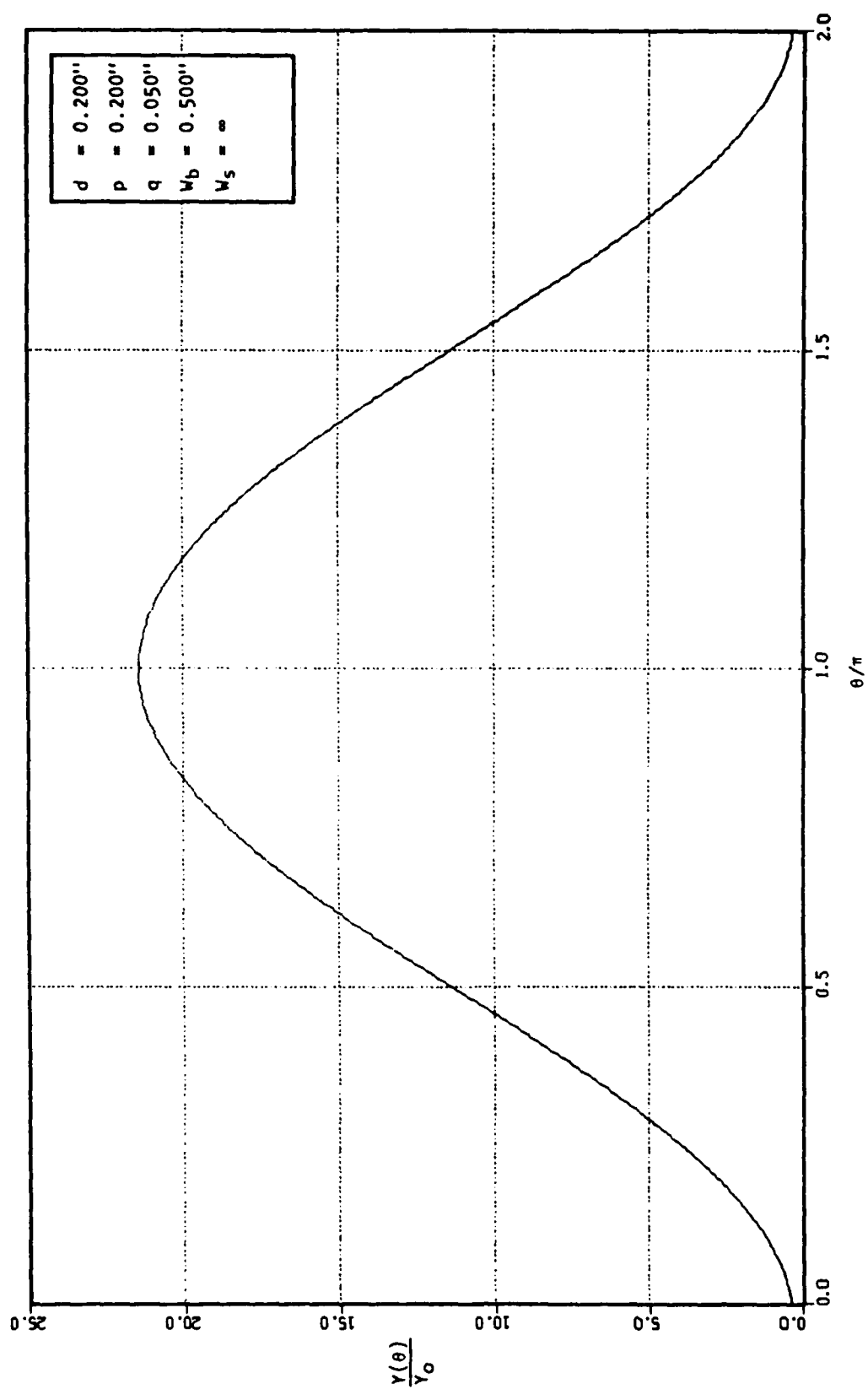


Fig. 2. Admittance function  $Y(\theta)$ .

$$\begin{aligned}
I^m(\phi) = & jY(\theta)[A_1 \cos \phi - A_2 \sin \phi] e^{-jm\theta} \\
& + jY(\theta + \pi)[A_3 \cos \phi - A_4 \sin \phi] e^{-jm(\theta+\pi)}
\end{aligned} \quad (12)$$

Referring to Fig. 1 and defining

$$\phi_0 = \omega h/c \quad (13)$$

the boundary conditions are given by

$$V^m_0(-\phi_0) = V^{m+1}_0(+\phi_0) = 0 \quad (14a)$$

$$I^m_0(+\phi_0) = I^{m+1}_0(-\phi_0) = 0 \quad (14b)$$

These specify that the current must be zero wherever a finger terminates in free space, and the voltage must be zero wherever a finger contacts a ground plane. As mentioned previously, the sidewalls, backwall, and sole are assumed to be at ground potential. Substituting Eqs. 4 and 12 into Eqs. 14 produces the linear system

$$\bar{M}\bar{a} = \bar{0} \quad (15)$$

where

$$\bar{a} = [A_1, A_2, A_3, A_4]^T \quad (16)$$

$$\Gamma = -1 \quad (17)$$

and  $\bar{M}$  is given by Eq. 18.

$$\bar{M} = \begin{bmatrix} -\sin \phi_0 & +\cos \phi_0 & -\Gamma^{m_0} \sin \phi_0 & +\Gamma^{m_0} \cos \phi_0 \\ +\sin \phi_0 & +\cos \phi_0 & +\Gamma^{m_0+1} \sin \phi_0 & +\Gamma^{m_0+1} \cos \phi_0 \\ +Y(\theta) \cos \phi_0 & -Y(\theta) \sin \phi_0 & +\Gamma^{m_0} Y(\theta+\pi) \cos \phi_0 & -\Gamma^{m_0} Y(\theta+\pi) \sin \phi_0 \\ +Y(\theta) \cos \phi_0 & +Y(\theta) \sin \phi_0 & +\Gamma^{m_0+1} Y(\theta+\pi) \cos \phi_0 & +\Gamma^{m_0+1} Y(\theta+\pi) \sin \phi_0 \end{bmatrix} \quad (18)$$

The dispersion characteristic states the conditions under which Eq. 15 is satisfied for arbitrary  $\bar{a}$ . These conditions are given by  $\det(\bar{M}) = 0$ . However, the final results are more easily obtained and more readily understood if  $\bar{M}$  is first transformed into  $\bar{M}'$ , using Gaussian elimination (which leaves the determinant unchanged), and the dispersion is then obtained from  $\det(\bar{M}') = 0$ . After some rearranging, this approach yields

$$\bar{M}' = \begin{bmatrix} +2 \sin \phi_0 & 0 & 0 & -2\Gamma^{m_0} \cos \phi_0 \\ +2Y(\theta) \cos \phi_0 & 0 & 0 & -2\Gamma^{m_0} Y(\theta+\pi) \sin \phi_0 \\ 0 & +2 \cos \phi_0 & -2\Gamma^{m_0} \sin \phi_0 & 0 \\ 0 & +2Y(\theta) \sin \phi_0 & -2\Gamma^{m_0} Y(\theta+\pi) \cos \phi_0 & 0 \end{bmatrix} \quad (19)$$

and subsequently,

$$\det(\bar{M}') = \det(\bar{M}) = 16\alpha\beta = 0 \quad (20)$$

where

$$\alpha = Y(\theta) \cos^2 \phi_0 - Y(\theta + \pi) \sin^2 \phi_0 \quad (21a)$$

$$\beta = Y(\theta) \sin^2 \phi_0 - Y(\theta + \pi) \cos^2 \phi_0 \quad (21b)$$

Equation 20 reveals two "independent" circuit modes whose dispersion characteristics are given by

$$1. \quad \alpha = 0 \quad \text{or} \quad \tan^2 \phi_0 = Y(\theta)/Y(\theta + \pi) \quad (22a)$$

$$A_2 = A_3 = 0 \quad (22b)$$

$$A_4 = +\Gamma^{\phi_0} \tan \phi_0 A_1 \quad (22c)$$

$$\begin{aligned} V^m(\phi) &= A_1 \sin \phi e^{-jm\theta} + A_4 \cos \phi e^{-jm(\theta+\pi)} \\ &= A_1 \left[ \sin \phi e^{-jm\theta} + \Gamma^{\phi_0} \tan \phi_0 \cos \phi e^{-jm(\theta+\pi)} \right] \end{aligned} \quad (22d)$$

$$\begin{aligned} I^m(\phi) &= jY(\theta)A_1 \cos \phi e^{-jm\theta} - jY(\theta + \pi)A_4 \sin \phi e^{-jm(\theta+\pi)} \\ &= jA_1 \left[ Y(\theta) \cos \phi e^{-jm\theta} - Y(\theta + \pi)\Gamma^{\phi_0} \tan \phi_0 \sin \phi e^{-jm(\theta+\pi)} \right] \end{aligned} \quad (22e)$$

$$2. \quad \beta = 0 \quad \text{or} \quad \cot^2 \phi_0 = Y(\theta)/Y(\theta + \pi) \quad (23a)$$

$$A_1 = A_4 = 0 \quad (23b)$$

$$A_3 = +\Gamma^m_0 \cot \phi_0 A_2 \quad (23c)$$

$$\begin{aligned} V^m(\phi) &= A_2 \cos \phi e^{-jm\theta} + A_3 \sin \phi e^{-jm(\theta+\pi)} \\ &= A_2 \left[ \cos \phi e^{-jm\theta} + \Gamma^m_0 \cot \phi_0 \sin \phi e^{-jm(\theta+\pi)} \right] \end{aligned} \quad (23d)$$

$$\begin{aligned} I^m(\phi) &= -jY(\theta)A_2 \sin \phi e^{-jm\theta} + jY(\theta + \pi)A_3 \cos \phi e^{-jm(\theta+\pi)} \\ &= jA_2 \left[ -Y(\theta) \sin \phi e^{-jm\theta} + Y(\theta + \pi)\Gamma^m_0 \cot \phi_0 \cos \phi e^{-jm(\theta+\pi)} \right] \end{aligned} \quad (23e)$$

The word independent is in quotes here because Eqs. 22 and 23 do not describe two distinct circuit modes, rather they describe the space harmonic structure of a single mode (see Chapter IV). The first pass-band of this mode is plotted in Fig. 3. Of particular interest are the primary space harmonics, i.e., the forward- and backward-wave components in the domain  $0 \leq \theta/\pi \leq 1$ .

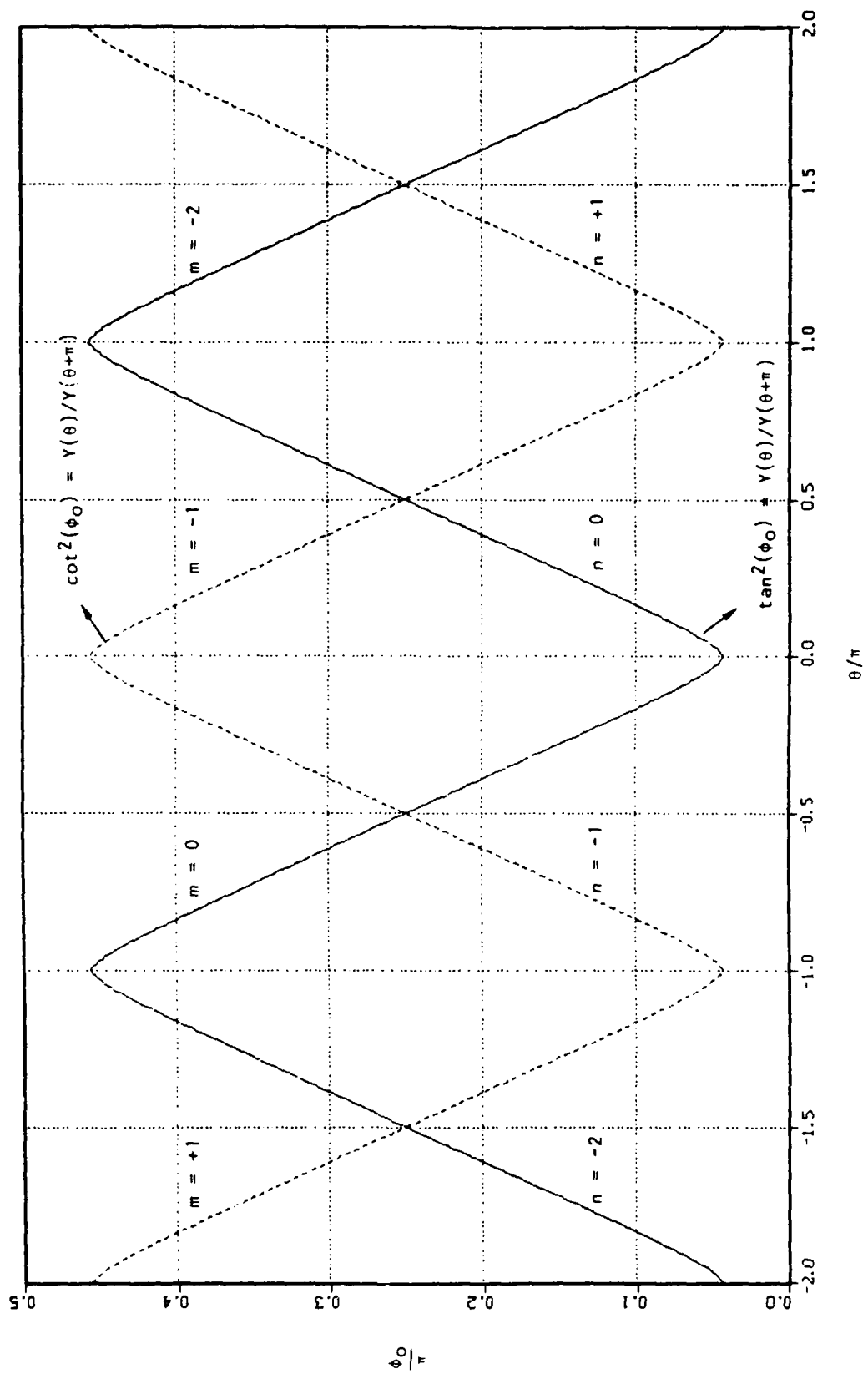


Fig. 3. First passband of the interdigital slow-wave circuit.

### C. Beam Coupling Impedance

The beam coupling impedance for the  $n$ th space harmonic as a function of position on the circuit is given by Pierce\* as

$$K_n(\theta, \phi) = \frac{|E_n|^2}{2\beta_n^2 P_{ta}} = \frac{l^2 E_n E_n^*}{2(\theta + n\pi)^2 v_g W_s} \quad (24)$$

where

$E_n$  =  $z$ -directed electric field at the position of the beam for the  $n$ th space harmonic

$\beta_n$  =  $(\theta + n\pi)/l$  = propagation constant for the  $n$ th space harmonic

$v_g$  = (magnitude of) group velocity for all space harmonics

$W_s$  = total stored energy per pitch

$P_{ta} = v_g W_s$  = time-averaged power flow on the circuit

and the star (\*) denotes complex conjugation. The leading factor of one-half arises from the time averaging of  $|E_n|^2$ . When averaged over a strip beam of width  $2b$ , Eq. 24 becomes

$$K_n(\theta) = \frac{1}{2\phi_b} \int_{-\phi_b}^{+\phi_b} K_n(\theta, \phi) d\phi \quad (25)$$

where  $\phi_b = \omega b/c$ . It is assumed that the beam is positioned at  $x = -d/2$ , i.e., just grazing the circuit at the interface between Regions 1 and 2 (see Fig. 1(b)).

### 1. Group Velocity $v_g$

The group velocity  $v_g$ , whose magnitude is of course the same for all space harmonics, is given by

$$v_g = \frac{d\omega}{d\beta} = \frac{d\omega}{d\theta} \frac{d\theta}{d\beta} \quad (26)$$

Since

$$\beta_n = \frac{(\theta + n\pi)}{l} \quad (27)$$

then,

$$d\theta/d\beta = l \quad (28)$$

The relationship between  $\omega$  and  $\theta$  is obtained from the dispersion relation as given by Eq. 22a. Using this equation and the identity

$$\frac{d(\tan^{-1} u)}{dx} = \frac{1}{1 + u^2} \frac{du}{dx} \quad (29)$$

gives

$$\frac{d\omega}{d\theta} = (c/2h)H(\theta) \quad (30)$$

where



$$H(\theta) = \frac{[Y(\theta + \pi)/Y(\theta)]^{1/2} Y'(\theta) - [Y(\theta)/Y(\theta + \pi)]^{1/2} Y'(\theta + \pi)}{[Y(\theta) + Y(\theta + \pi)]} \quad (31)$$

and a prime (') denotes differentiation with respect to  $\theta$ . Thus,

$$v_g = (lc/2h) H(\theta) \quad (32)$$

This result is easily derived or can be obtained from Walling's Eq. 16.<sup>2</sup>

## 2. Stored Energy Per Pitch $W_s$

The stored energy per pitch is determined by dividing the stored energy between adjacent fingers by the circuit pitch,  $l$ . The stored energy between adjacent fingers is given by the total power flow along a finger multiplied by the time it takes to traverse a finger, which can be expressed as the finger length,  $2h$ , divided by the speed of light,  $c$ . Thus, for TEM waves,

$$W_s = 2hP_{ta}/lc \quad (33)$$

where

$P_{ta}$  = time-averaged power flow along the fingers

$$= \text{Re}[VI^*]/2$$

$$= \text{Re}[V_\theta I_\theta^*]/2 + \text{Re}[V_{\theta+\pi} I_{\theta+\pi}^*]/2$$

$$= P_\theta + P_{\theta+\pi} \quad (34)$$

The contributions from the  $\theta$  and  $\theta + \pi$  components of  $V$  and  $I$  can be summed separately, since these harmonics are uncoupled from one another. Using Eqs. 22a, 22d, and 22e in Eq. 34 yields

$$P_{\theta} = P_{\theta+\pi} = A_1^2 Y(\theta) [1 - 1]/8 \quad (35)$$

At this point, it must be recognized that the first term in the brackets in Eq. 35 is the TEM forward-wave contribution to the power flow, and the second term is the corresponding backward-wave contribution. To determine the total stored energy, the magnitude of the power flow due to each component must be summed. Therefore,

$$P_{\theta} = P_{\theta+\pi} + A_1^2 Y(\theta)/4 \quad (36)$$

and the final result is

$$W_s = \frac{h}{1c} Y(\theta) A_1^2 \quad (37)$$

### 3. Electric Field Distribution $E_n E_n^*$

The electric field distribution,  $E_n E_n^*$ , is determined by following the procedure outlined by Fletcher.<sup>1</sup> To begin, it is assumed that the electric field between the fingers in Region 1 (see Fig. 1(b)) is uniform. The field can then be expressed as the voltage difference between two adjacent fingers divided by the distance  $q$  between them. Over one period of the circuit, this is given by

$$E_1 = \begin{cases} (V^{m+1} - V^m)/q, & m\ell + (p/2) < z < (m+1)\ell - (p/2) \\ (V^m - V^{m-1})/q, & (m-1)\ell + (p/2) < z < m\ell - (p/2) \\ 0, & (m-1)\ell < z < (m-1)\ell + (p/2) \\ 0, & m\ell - (p/2) < z < m\ell + (p/2) \\ 0, & (m+1)\ell - (p/2) < z < (m+1)\ell \end{cases} \quad (38)$$

Because Eqs. 22d and 23d describe the same circuit mode, either can be used here to determine  $E_1$ . Equation 22d is substituted into Eq. 38 to give

$$E_1 = \begin{cases} E_\theta \sin \phi e^{-j[m+(1/2)]\theta} + E_{\theta+\pi} \cos \phi e^{-j[m+(1/2)][\theta+\pi]} & m\ell + (p/2) < z < (m+1)\ell - (p/2) \\ E_\theta \sin \phi e^{-j[m-(1/2)]\theta} + E_{\theta+\pi} \cos \phi e^{-j[m-(1/2)][\theta+\pi]} & (m-1)\ell + (p/2) < z < m\ell - (p/2) \\ 0, & (m-1)\ell < z < (m-1)\ell + (p/2) \\ 0, & m\ell - (p/2) < z < m\ell + (p/2) \\ 0, & (m+1)\ell - (p/2) < z < (m+1)\ell \end{cases} \quad (39)$$

where

$$E_{\theta} = -j2A_1 q^{-1} \sin(\theta/2) \quad (40a)$$

$$E_{\theta+\pi} = -j2A_1 q^{-1} \tan \phi_0 \cos(\theta/2) \quad (40b)$$

The electric fields in Regions 2 and 3 are represented by Fourier expansions over one period,  $L = 2\ell$ , which satisfy the boundary conditions imposed by the sole and backwall, respectively. These are given by

$$\begin{aligned} E_{2,3} &= \sum E_n \\ &= \sum \left[ F_n \sin \phi + G_n \cos \phi \right] \frac{\sinh[(\theta + n\pi)(w_{s,b} \pm x)/2\ell] e^{-j(\theta+n\pi)z/2\ell}}{\sinh[(\theta + n\pi)w_{s,b}/2\ell]} \end{aligned} \quad (41)$$

where again the summation is from  $n = -\infty$  to  $n = +\infty$ . It is also assumed that Region 1 is infinitesimally thin, so that at  $x = 0$ ,

$$(E_2)_{x=0} = (E_3)_{x=0} = E_1 \quad (42)$$

Substituting Eqs. 39 and 41 into Eq. 42, multiplying both sides of the resulting equation by  $e^{+j(\theta+n\pi)z/2\ell}$ , and integrating over one period gives

$$F_n = \begin{cases} 0 & n \text{ odd} \\ \frac{E_{\theta} q \Gamma^{n/2}}{\ell} \frac{\sin [(\theta + n\pi)q/2\ell]}{[(\theta + n\pi)q/2\ell]} & n = \text{even} \end{cases} \quad (43a)$$

$$G_n = \begin{cases} \frac{E_{\theta+\pi} q \Gamma^{m_0 + [(n-1)/2]}}{\ell} \frac{\sin [(\theta + n\pi)q/2\ell]}{[(\theta + n\pi)q/2\ell]} & n \text{ odd} \\ 0 & n \text{ even} \end{cases} \quad (43b)$$

where the orthogonality of sine and cosine has been used. Using Eqs. 43 in Eq. 41 and taking  $x = 0$  yields

$$E_n = (E_{2,3})_{x=0} = \begin{cases} G_n \cos \phi e^{-j(\theta+n\pi)z/2\ell} & n \text{ odd} \\ F_n \sin \phi e^{-j(\theta+n\pi)z/2\ell} & n \text{ even} \end{cases} \quad (44)$$

The space harmonics of interest are those in the domains  $0 \leq \theta/\pi \leq 1$  ("primary domain") and  $1 \leq \theta/\pi \leq 2$  ("secondary domain"). These are the  $n = 0$  and  $n = +1$  forward-wave harmonics and the  $m = -1$  and  $m = -2$  backward-wave harmonics. The electric field distributions for these components are given by

$$E_0 E_0^* = \frac{4A_1^2}{l^2} \sin^2 (\theta/2) \frac{\sin^2 [\theta q/2l]}{[\theta q/2l]^2} \sin^2 \phi \quad (45a)$$

$$E_{+1} E_{+1}^* = \frac{4A_1^2}{l^2} \tan^2 \phi_0 \cos^2 (\theta/2) \frac{\sin^2 [(\theta + \pi)q/2l]}{[(\theta + \pi)q/2l]^2} \cos^2 \phi \quad (45b)$$

$$E_{-1} E_{-1}^* = \frac{4A_1^2}{l^2} \tan^2 \phi_0 \cos^2 (\theta/2) \frac{\sin^2 [(\pi - \theta)q/2l]}{[(\pi - \theta)q/2l]^2} \cos^2 \phi \quad (45c)$$

$$E_{-2} E_{-2}^* = \frac{4A_1^2}{l^2} \sin^2 (\theta/2) \frac{\sin^2 [(2\pi - \theta)q/2l]}{[(2\pi - \theta)q/2l]^2} \sin^2 \phi \quad (45d)$$

Those components which possess a  $\sin^2 \phi$  dependence have been dubbed "edge" modes. Their regions of greatest field intensity, and therefore of greatest coupling, are at the edges of the circuit, i.e., at the ends of the fingers. Similarly, those which possess a  $\cos^2 \phi$  dependence have been dubbed "center" modes.

#### 4. Final Expressions for Beam Coupling Impedance

Using Eqs. 32, 37, and 45 along with the identities

$$\frac{1}{2\phi_b} \int_{-\phi_b}^{+\phi_b} \frac{\sin^2 \phi}{\cos^2 \phi} d\phi = \frac{1}{2} + \frac{\sin(2\phi_b)}{4\phi_b} \quad (46)$$

in Eq. 25 yields

$$K_i = K_i^1 * K_i^2 \quad i = 0, +1, -1, -2 \quad (47)$$

$$K_{0,-1}^1 = K_{-2,+1}^1 = \frac{1}{2} \mp \frac{\sin(2\phi_b)}{4\phi_b} \quad (48)$$

$$K_0^2 = \frac{4 \sin^2(\theta/2)}{\theta^2 H(\theta)Y(\theta)} \frac{\sin^2[\theta q/2l]}{[\theta q/2l]^2} \quad (49a)$$

$$K_{+1}^2 = \frac{4 \tan^2 \phi_0}{(\theta + \pi)^2 H(\theta)Y(\theta)} \cos^2(\theta/2) \frac{\sin^2[(\theta + \pi)q/2l]}{[(\theta + \pi)q/2l]^2} \quad (49b)$$

$$K_{-1}^2 = \frac{4 \tan^2 \phi_0}{(\pi - \theta)^2 H(\theta)Y(\theta)} \cos^2(\theta/2) \frac{\sin^2[(\pi - \theta)q/2l]}{[(\pi - \theta)q/2l]^2} \quad (49c)$$

$$K_{-2}^2 = \frac{4 \sin^2(\theta/2)}{(2\pi - \theta)^2 H(\theta)Y(\theta)} \frac{\sin^2[(2\pi - \theta)q/2l]}{[(2\pi - \theta)q/2l]^2} \quad (49d)$$

In these expressions,  $K^1$  represents the effect of the electric field distribution on the magnitude of the beam coupling impedance. It is the end result of the integration of the  $\phi$  dependence of the electric field over the total beamwidth.  $K^2$  is the composite of all other factors. These beam coupling impedances are plotted in Figs. 4 and 5 for  $\phi_b = \phi_0$ , i.e., for a beam which spans the entire width of the circuit. A detailed discussion of these results is reserved until Chapter IV.

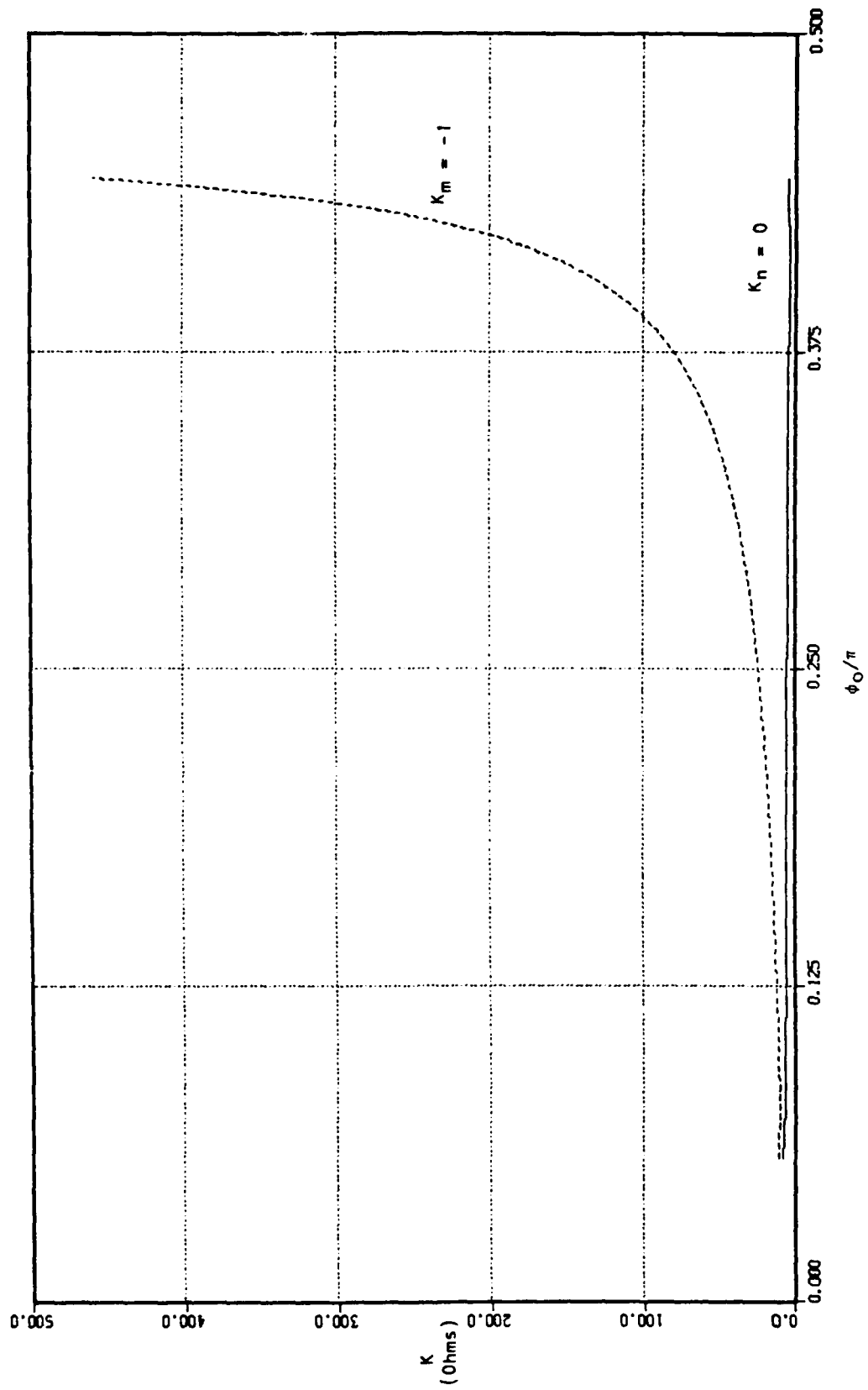


Fig. 4a. Beam coupling impedance for the primary interdigital space harmonics.



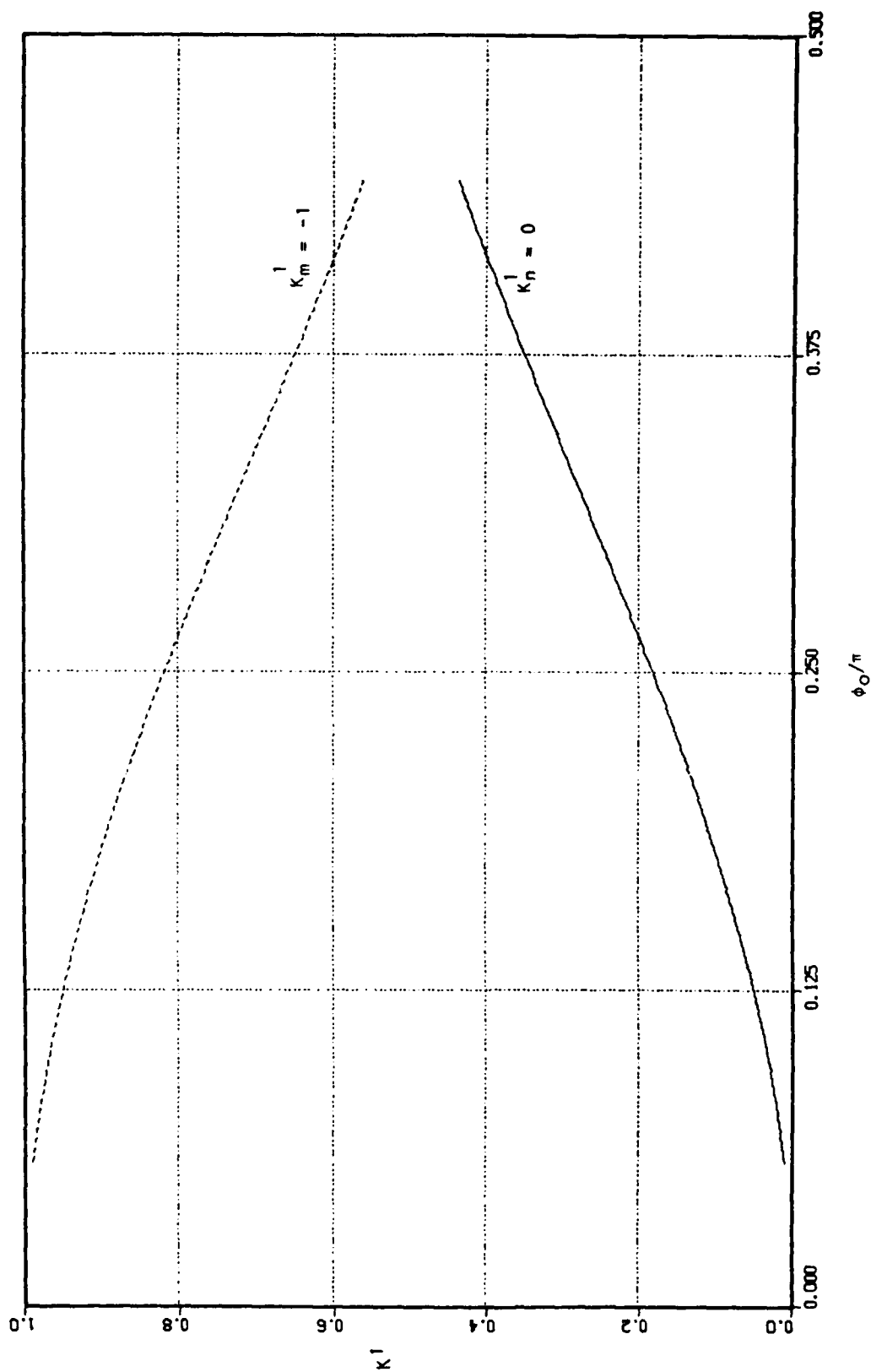


Fig. 4b.  $K^1$  for the primary interdigital space harmonics.

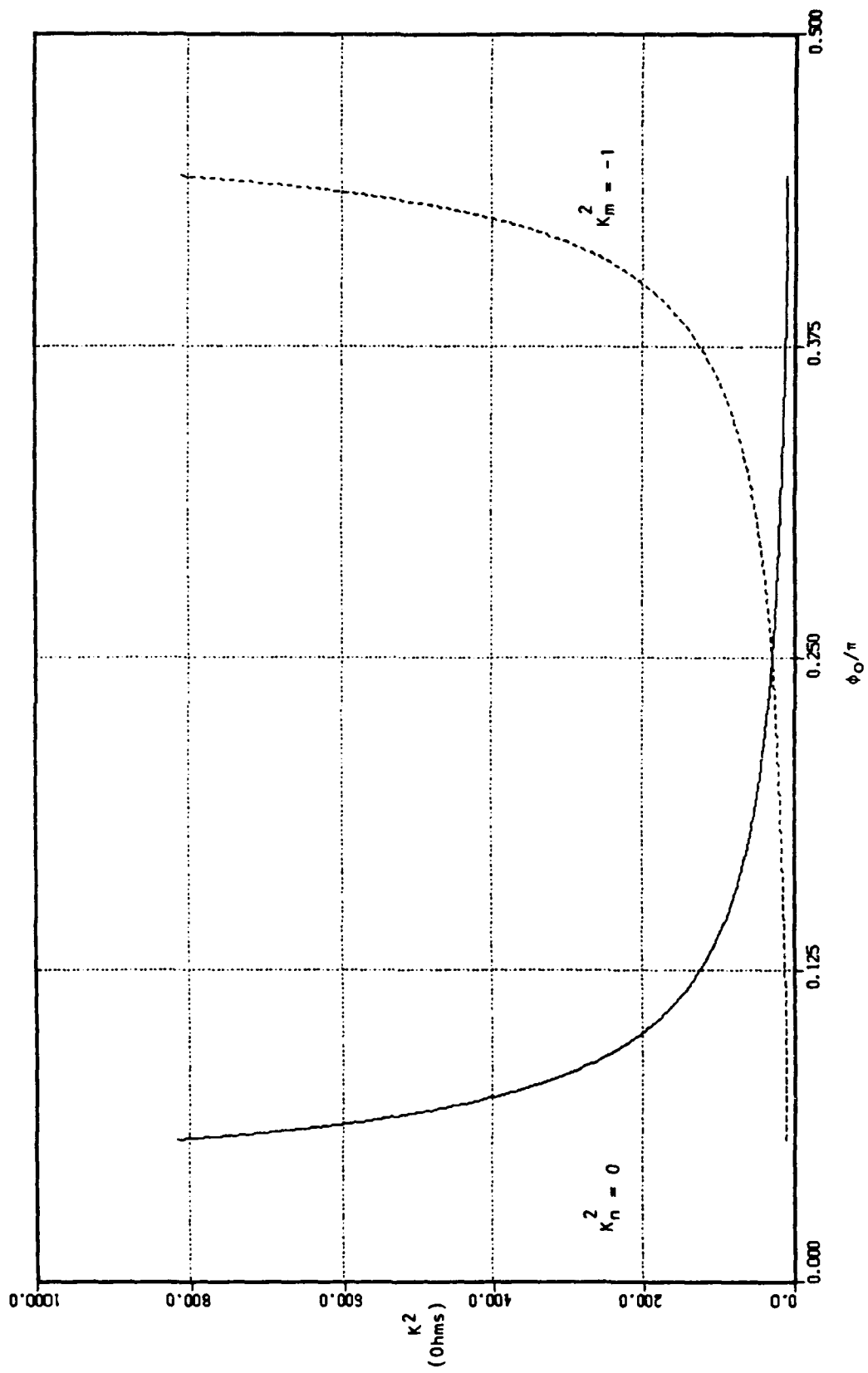


Fig. 4c.  $K^2$  for the primary interdigital space harmonics.

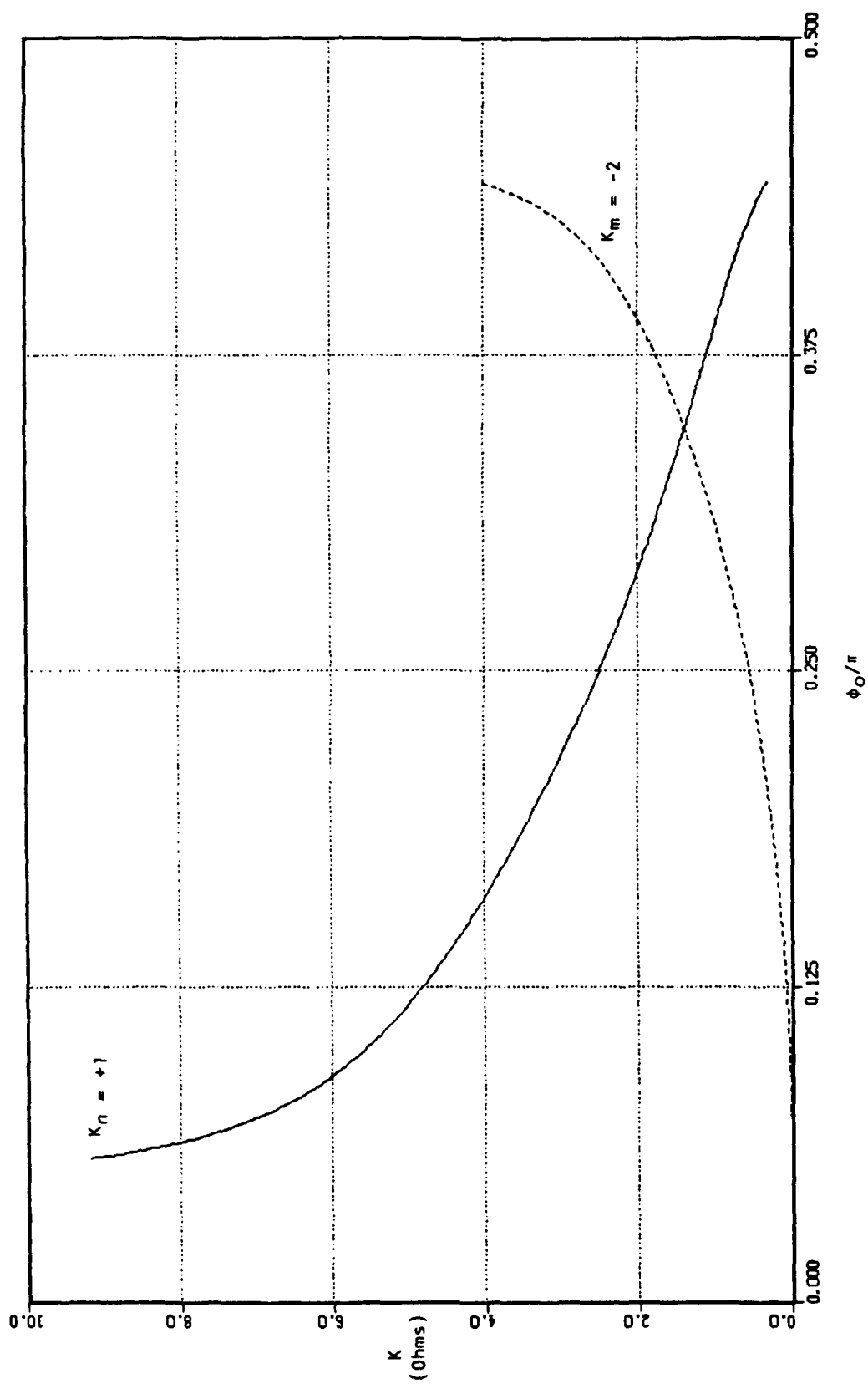


Fig. 5a. Beam coupling impedance for the secondary interdigital space harmonics.

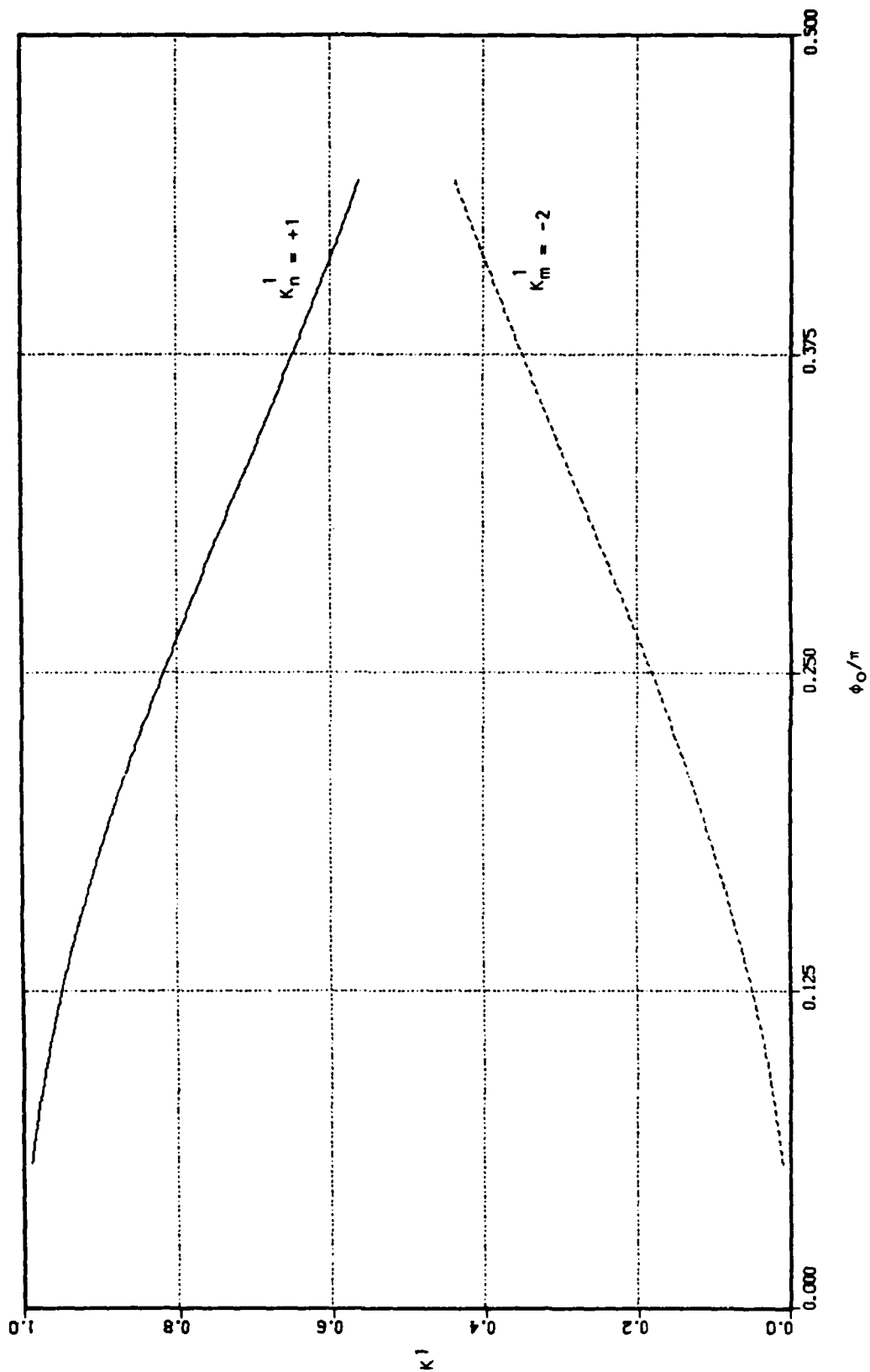


Fig. 5b.  $K'$  for the secondary interdigital space harmonics.

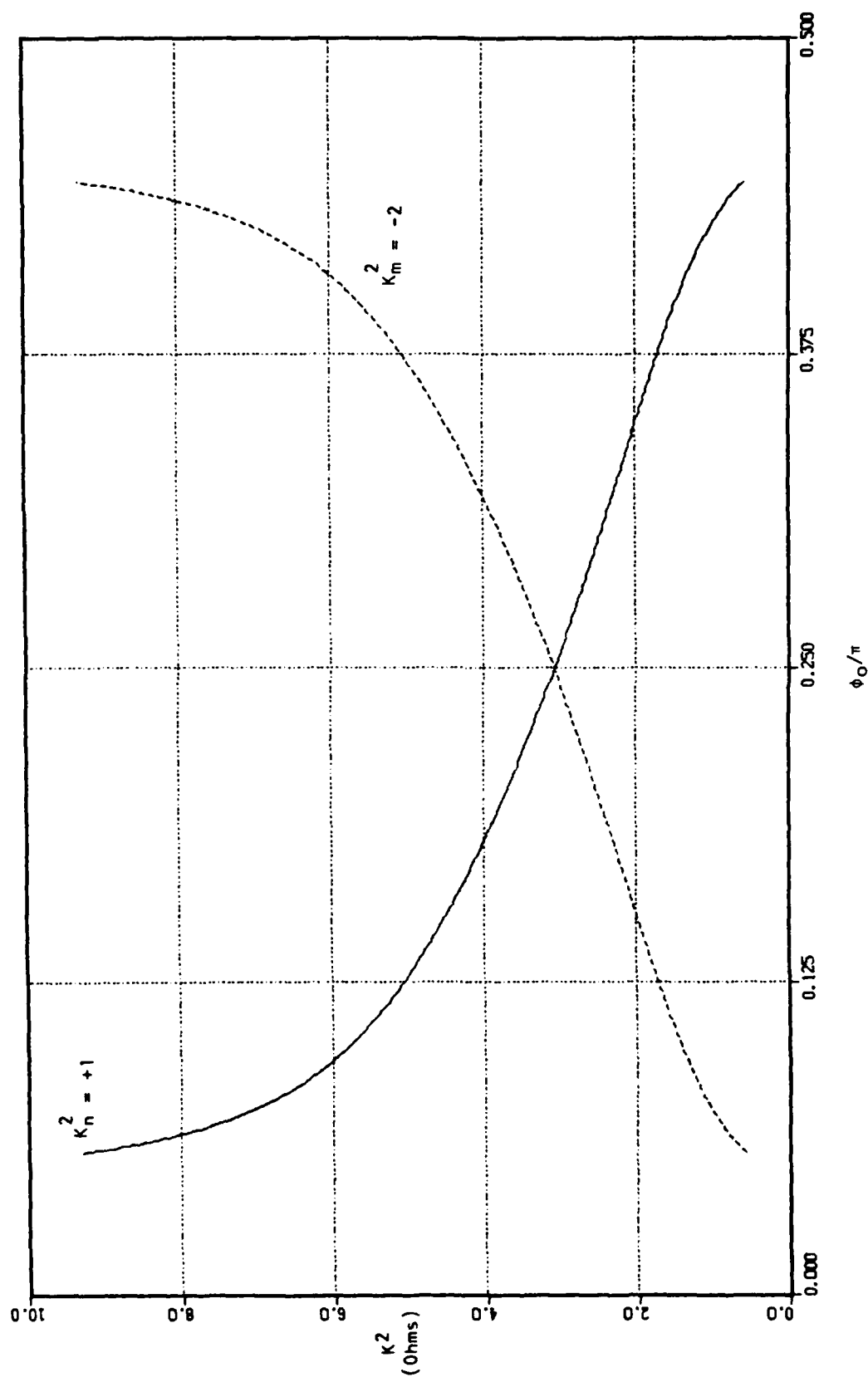


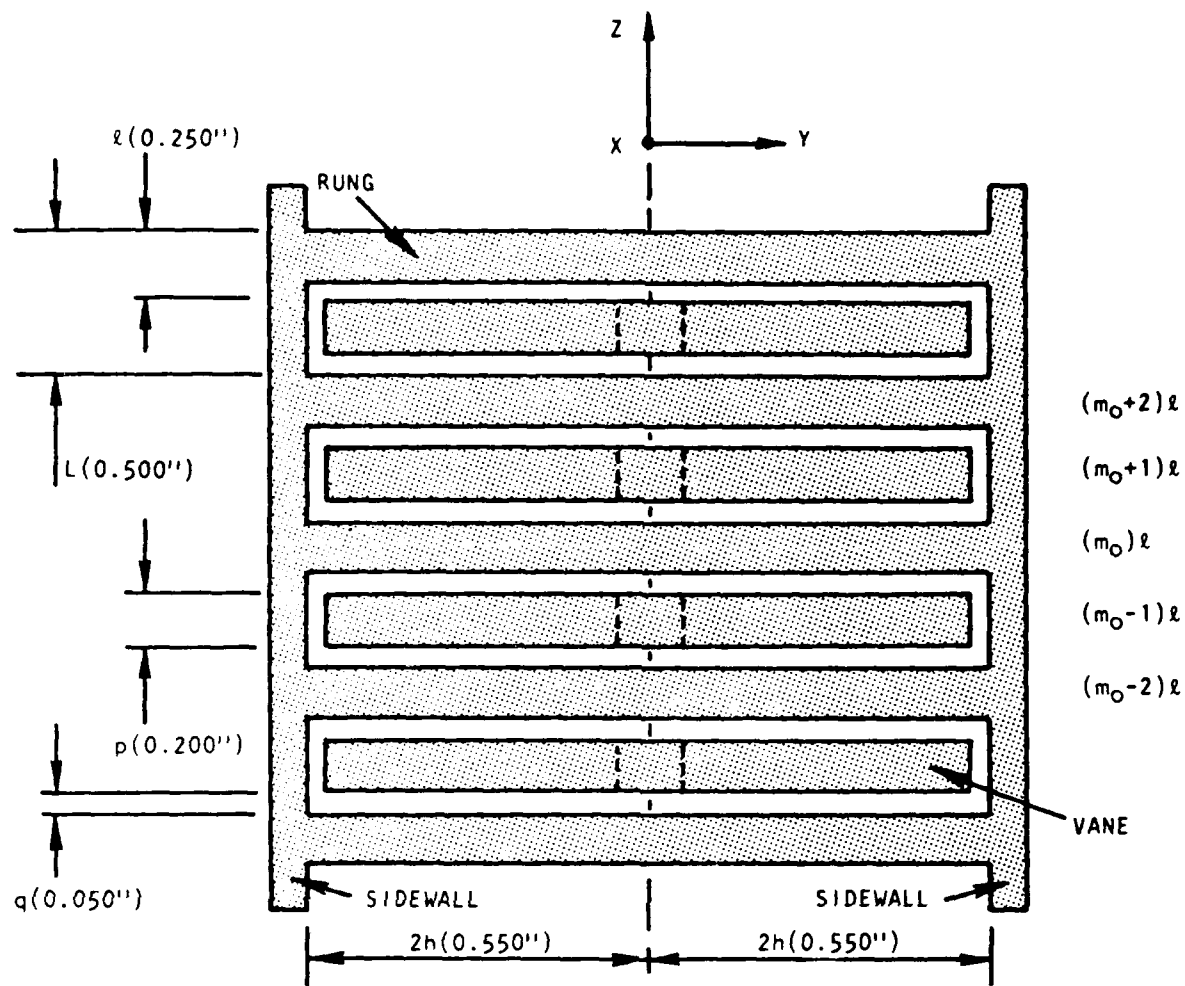
Fig. 5c.  $K^2$  for the secondary interdigital space harmonics.

### III. ANALYSIS OF THE VANE-LOADED LADDER SLOW-WAVE CIRCUIT

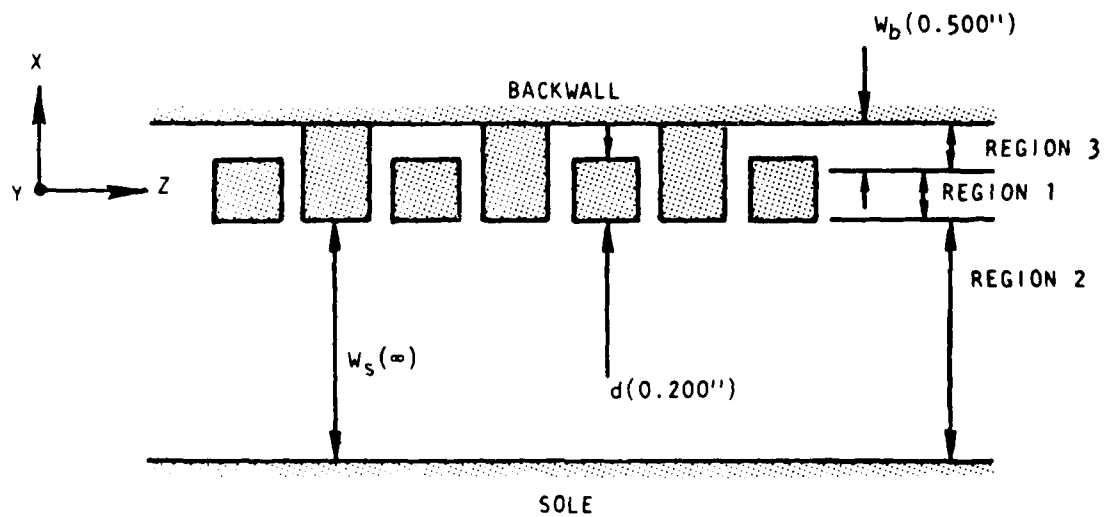
A close examination of the results of the previous chapter indicates that a useful amplifier circuit would be one which provides the instantaneous bandwidth of the interdigital line, while reversing the impedance behavior of the primary space harmonics (this will be discussed in detail in the following chapter). The vane-loaded ladder circuit presented in this chapter is a circuit designed to serve in this capacity.

#### A. Circuit Illustration and Description

The circuit under consideration is shown in Fig. 6. It is also a planar circuit composed of two types of circuit elements which alternate one after the other in the direction of propagation  $Z$ . As before, the pitch,  $l$ , is the center-to-center distance between adjacent fingers of opposite type, and the period,  $L = 2l$ , is the similarly defined distance between adjacent fingers of the same type. Elements of the first type are fingers of length  $4h$  which extend away from the centerline on both sides. These elements are attached to the sidewalls at both ends and are not connected to the backwall at the centerline. Elements of the second type are assumed to have the same length, but are connected to the backwall at the centerline and are not attached to the sidewalls. For convenience, elements of the first type are called rungs (because of their likeness to the rungs of a ladder) and elements of the second type are called vanes; hence, the name vane-loaded ladder. As with the interdigital line, the circuit may also be loaded by the presence of a



(a) Top view.



(b) Side view.

Fig. 6. Vane-loaded ladder slow-wave circuit.

sole which is at ground potential along with the backwall and sidewalls. In a traveling-wave tube, a strip beam of width  $2b$  would be injected between the circuit and the sole.

The conception of the circuit is more easily understood if it is viewed as a joining of two adjacent interdigital lines (without a "sidewall" down the center), as shown in Fig. 7. The purpose of such a joining is to propagate interdigital line modes to either side of the centerline. This preserves the interdigital line dispersion, while reversing the electric field distributions (from edge mode to center mode and vice versa) for the primary space harmonics. The latter feature is designed to alter the impedance behavior through its impact on the field distribution factor  $K^1$ .

#### B. Dispersion Characteristics

The technique used here to derive the dispersion characteristic for the vane-loaded ladder line is nearly identical to that employed for the interdigital line. The difference between the two is not in the fundamentals of the formulation, but in how it is applied. In the interdigital line analysis, the entire circuit was considered as a single region, i.e., just one voltage was defined over the entire length of the fingers. This was appropriate since it provided four unknowns,  $A_1$ - $A_4$ , for which to solve using the four boundary conditions. The vane-loaded ladder, however, imposes an additional constraint: the voltage must go to zero at the center of the vanes where they connect to the backwall. Treating this circuit as a single region would yield an overdetermined system of five boundary conditions for only four



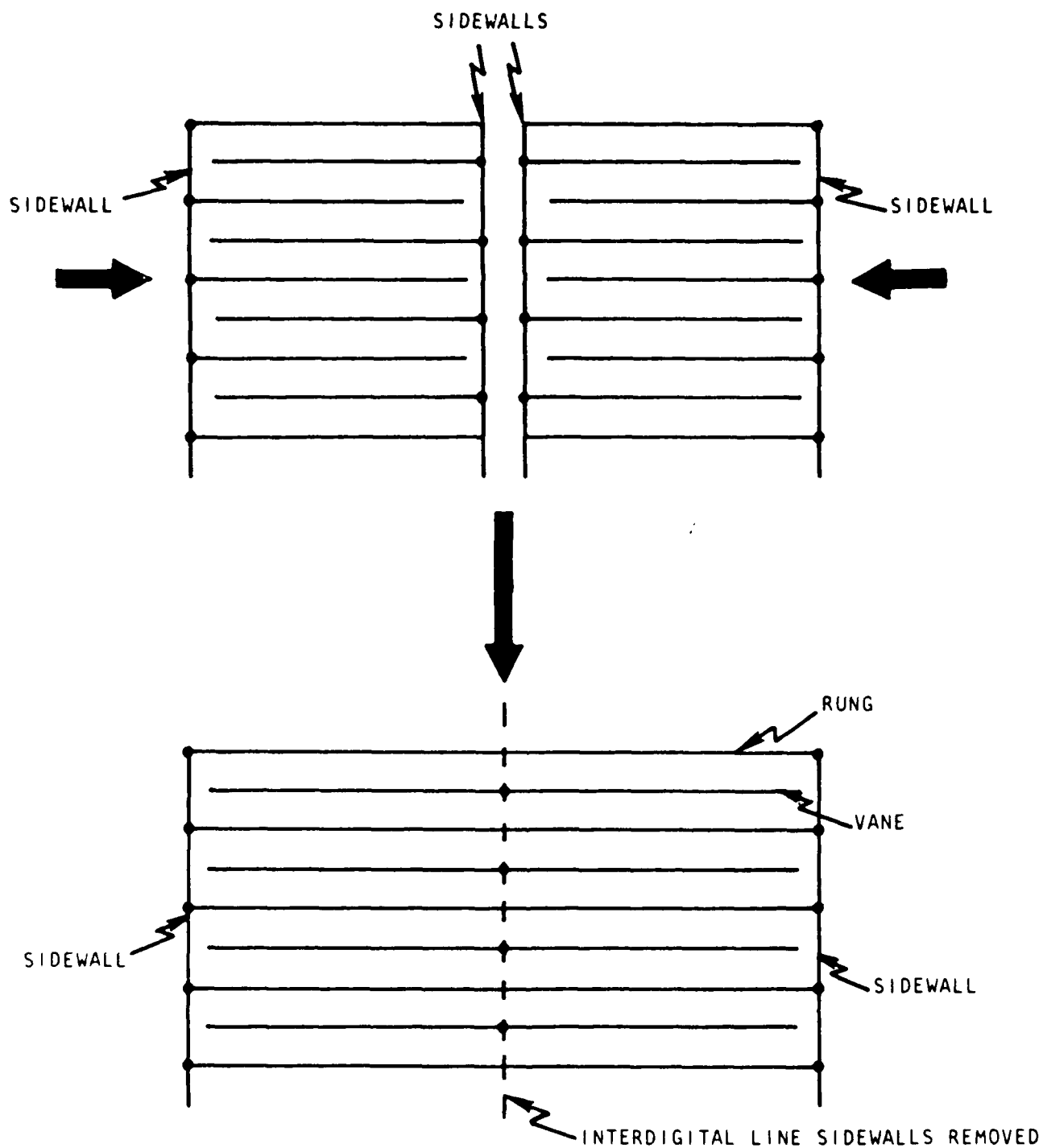


Fig. 7. Vane-loaded ladder as a consolidation of two interdigital slow-wave circuits.

unknowns. To avoid this, the circuit is bisected at the centerline into two equal regions. This is shown in Fig. 8. Each region has its own voltage and admittance function, both of which are defined to exist only in that region. This gives a total of eight unknowns, leaving a need for three additional boundary conditions. These additional conditions are obtained by requiring that the voltage and current on the rungs and the voltage on the vanes be continuous across the centerline. It is not necessary to force current continuity on the vanes, since any disparity at this point would be considered as current flowing into the backwall.

The voltage in a given region is naturally a function of position, and normally the position in either region is referenced to the same origin or centerline. If this is done here, however, the dispersion assumes a form from which the circuit modes are nearly impossible to distinguish. To eliminate this problem, the positional dependence of the circuit quantities is referenced to the centerline of their respective regions rather than the centerline of the circuit. This causes no loss of generality. In fact, it can be shown using simple trigonometric identities that the frame of reference change is just absorbed into the voltage coefficients  $B_1$ - $B_8$ . Referencing Fig. 8 and defining,

$$\phi_0 = wh/c \quad (50)$$

$$\phi_{01} = -\phi_0 = \text{coordinate of Region I centerline} \quad (51)$$

$$\phi_{02} = +\phi_0 = \text{coordinate of Region II centerline} \quad (52)$$

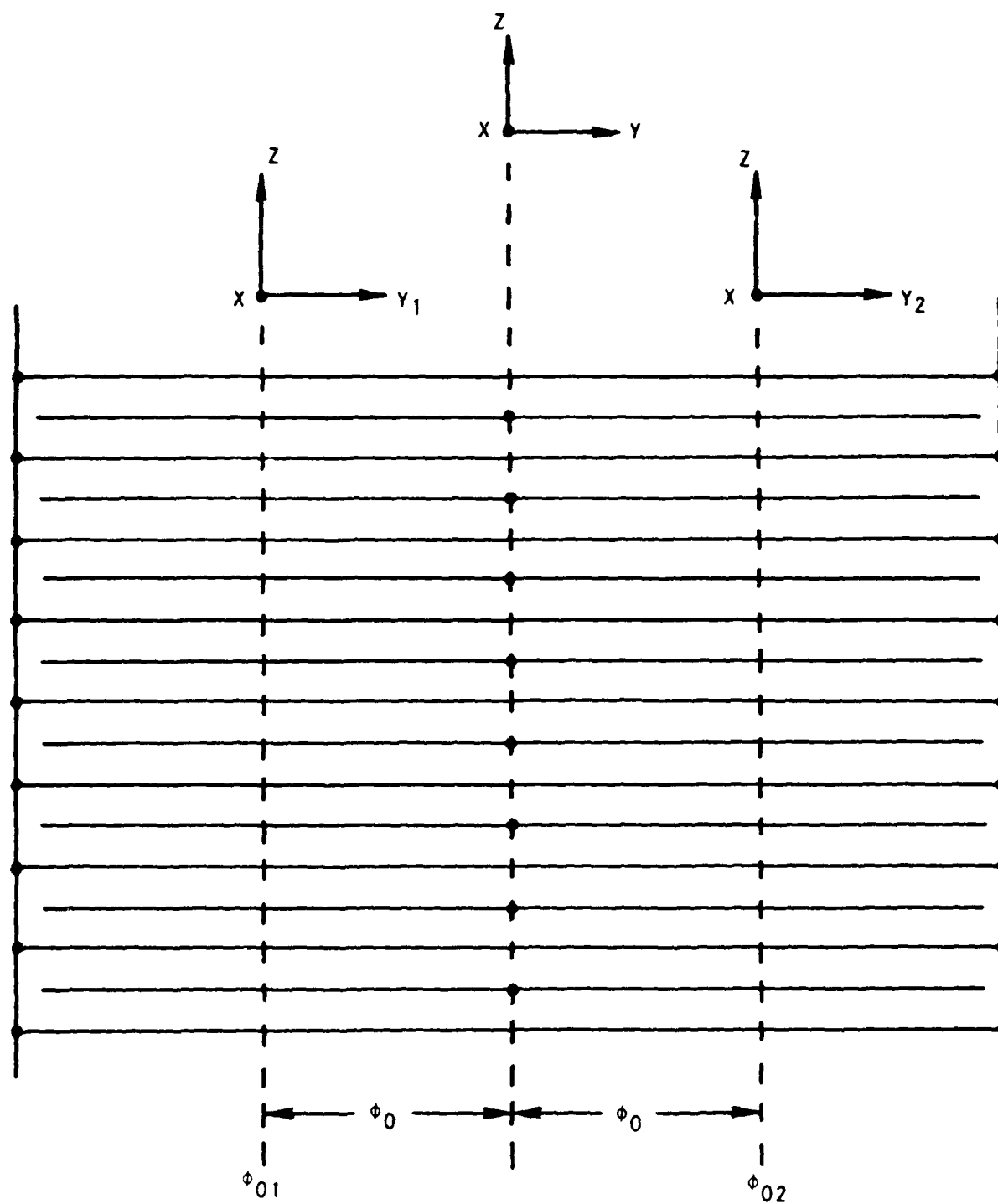


Fig. 8. Vane-loaded ladder bisected into two equal regions.

the voltages in each region at a given position on the mth finger are given by

$$V_1^m(\phi_1) = \left[ B_1 \sin \phi_1 + B_2 \cos \phi_1 \right] e^{-jm\theta} + \left[ B_3 \sin \phi_1 + B_4 \cos \phi_1 \right] e^{-jm(\theta+\pi)} \quad (53a)$$

$$V_2^m(\phi_2) = \left[ B_5 \sin \phi_2 + B_6 \cos \phi_2 \right] e^{-jm\theta} + \left[ B_7 \sin \phi_2 + B_8 \cos \phi_2 \right] e^{-jm(\theta+\pi)} \quad (53b)$$

where

$$\phi_1 = \phi - \phi_{01} = \phi + \phi_0 \quad (54a)$$

$$\phi_2 = \phi - \phi_{02} = \phi - \phi_0 \quad (54b)$$

The currents are obtained using Eq. 11 and are given by

$$I_1^m(\phi_1) = jY(\theta) \left[ C_1 \cos \phi_1 - C_2 \sin \phi_1 \right] e^{-jm\theta} + jY(\theta + \pi) \left[ C_3 \cos \phi_1 - C_4 \sin \phi_1 \right] e^{-jm(\theta+\pi)} \quad (55a)$$

$$I_2^m(\phi_2) = jY(\theta) \left[ C_5 \cos \phi_2 - C_6 \sin \phi_2 \right] e^{-jm\theta} + jY(\theta + \pi) \left[ C_7 \cos \phi_2 - C_8 \sin \phi_2 \right] e^{-jm(\theta+\pi)} \quad (55b)$$

For simplicity, it has been assumed that the circuit dimensions and wall spacings are identical in the two regions, making the corresponding admittance functions indistinguishable from one another.

Assuming the  $m_0$  finger is a rung, the boundary conditions are given by

$$1. \quad V_1^{m_0} (\phi_1 = -\phi_0) = 0 \quad (56a)$$

$$2. \quad V_2^{m_0} (\phi_2 = +\phi_0) = 0 \quad (56b)$$

$$3. \quad V_1^{m_0+1} (\phi_1 = +\phi_0) = 0 \quad (56c)$$

$$4. \quad V_2^{m_0+1} (\phi_2 = -\phi_0) = 0 \quad (56d)$$

$$5. \quad I_1^{m_0+1} (\phi_1 = -\phi_0) = 0 \quad (56e)$$

$$6. \quad I_2^{m_0+1} (\phi_2 = +\phi_0) = 0 \quad (56f)$$

$$7. \quad V_1^{m_0} (\phi_1 = +\phi_0) - V_2^{m_0} (\phi_2 = -\phi_0) = 0 \quad (56g)$$

$$8. \quad I_1^{m_0} (\phi_1 = +\phi_0) - I_2^{m_0} (\phi_2 = -\phi_0) = 0 \quad (56h)$$

As before, these specify that the current must be zero wherever a finger terminates in free space, and the voltage must be zero wherever a finger contacts a ground plane. The last three are those which result from the continuity requirements (rather than explicitly forcing voltage

continuity where the vanes meet the backwall, it is done implicitly by setting both voltages to the same value, namely, zero. Substituting Eqs. 53 and 55 into Eqs. 56 yields the linear system,

$$\bar{M}\bar{b} = \bar{0} \quad (57)$$

where

$$\bar{b} = [B_1, B_2, B_3, B_4, B_5, B_6, B_7, B_8]^T \quad (58)$$

$$\Gamma = -1 \quad (59)$$

and  $\bar{M}$  is given by Eq. 60.

$-\sin \phi_0$	$+\cos \phi_0$	$-\Gamma^m_0 \sin \phi_0$	$+\Gamma^m_0 \cos \phi_0$	0	0	0	0
0	0	0	0	$+\sin \phi_0$	$+\cos \phi_0$	$+\Gamma^m_0 \sin \phi_0$	$+\Gamma^m_0 \cos \phi_0$
$+\gamma(\theta)\cos \phi_0$	$+\gamma(\theta)\sin \phi_0$	$+\gamma(\theta+\pi)\Gamma^{m+1}_0 \cos \phi_0$	$+\gamma(\theta+\pi)\Gamma^{m+1}_0 \sin \phi_0$	0	0	0	0
0	0	0	0	$+\gamma(\theta)\cos \phi_0$	$-\gamma(\theta)\sin \phi_0$	$+\gamma(\theta+\pi)\Gamma^{m+1}_0 \cos \phi_0$	$-\gamma(\theta+\pi)\Gamma^{m+1}_0 \sin \phi_0$
$+\sin \phi_0$	$+\cos \phi_0$	$+\Gamma^{m+1}_0 \sin \phi_0$	$+\Gamma^{m+1}_0 \cos \phi_0$	0	0	0	0
0	0	0	0	$-\sin \phi_0$	$+\cos \phi_0$	$-\Gamma^{m+1}_0 \sin \phi_0$	$+\Gamma^{m+1}_0 \cos \phi_0$
$+\sin \phi_0$	$+\cos \phi_0$	$+\Gamma^m_0 \sin \phi_0$	$+\Gamma^m_0 \cos \phi_0$	$+\sin \phi_0$	$-\cos \phi_0$	$+\Gamma^m_0 \sin \phi_0$	$-\Gamma^m_0 \cos \phi_0$
$+\gamma(\theta)\cos \phi_0$	$-\gamma(\theta)\sin \phi_0$	$+\gamma(\theta+\pi)\Gamma^m_0 \cos \phi_0$	$-\gamma(\theta+\pi)\Gamma^m_0 \sin \phi_0$	$-\gamma(\theta)\cos \phi_0$	$-\gamma(\theta)\sin \phi_0$	$-\gamma(\theta+\pi)\Gamma^m_0 \cos \phi_0$	$-\gamma(\theta+\pi)\Gamma^m_0 \sin \phi_0$

(60)

$\bar{M} =$

Satisfying Eq. 57 for arbitrary  $\bar{b}$  requires that  $\det(\bar{M}) = 0$ . Similar to the technique used in Chapter II,  $\bar{M}$  is first reduced to a fourth-order matrix  $\bar{M}'$  using Gaussian elimination, and the dispersion is then obtained from

$$\det(\bar{M}') = \det(\bar{M}) = 8\alpha\beta \left[ \sin^2 \phi_0 - \cos^2 \phi_0 \right] \left[ Y(\theta) + Y(\theta + \pi) \right] = 0 \quad (61)$$

where

$$\alpha = Y(\theta) \cos \phi_0 - Y(\theta + \pi) \tan \phi_0 \sin \phi_0 \quad (62)$$

$$\beta = Y(\theta) \sin \phi_0 - Y(\theta + \pi) \tan \phi_0 \cos \phi_0 \quad (63)$$

This dispersion characteristic reveals two (truly) independent circuit modes. The first mode is a set of resonances which occur at  $\phi_0 = n\pi/4$ ,  $n = 0, 1, 2, 3, \dots$ . These are the frequencies at which the ladder resonates, i.e., at which the total length of the rungs is equal to an integral number of half-wavelengths. Equation 61 shows only the  $\phi_0 = \pi/4 \pm n\pi/2$  resonances because the  $\phi_0 = n\pi/2$  resonances are lost in the reduction of the original, eighth-order system. The second independent mode is exactly the interdigital line mode discussed in the previous chapter. As before, both the  $\alpha = 0$  and  $\beta = 0$  modes of Eq. 61 are actually describing the space harmonic structure of a single circuit mode. They are given by



$$1. \quad \alpha = 0 \text{ or } \tan^2 \phi_0 = \frac{Y(\theta)}{Y(\theta + \pi)} \quad (64a)$$

$$B_2 = B_3 = B_6 = B_7 = 0 \quad (64b)$$

$$B_4 = B_8 = \Gamma^m_0 \tan \phi_0 B_1 \quad (64c)$$

$$B_5 = -B_1 \quad (64d)$$

$$V_1^m(\phi_1) = B_1 \left[ \sin \phi_1 e^{-jm\theta} + \Gamma^m_0 \tan \phi_0 \cos \phi_1 e^{-jm(\theta+\pi)} \right] \quad (64e)$$

$$I_1^m(\phi_1) = jB_1 \left[ Y(\theta) \cos \phi_1 e^{-jm\theta} - Y(\theta + \pi) \Gamma^m_0 \tan \phi_0 \sin \phi_1 e^{-jm(\theta+\pi)} \right] \quad (64f)$$

$$V_2^m(\phi_2) = B_1 \left[ -\sin \phi_2 e^{-jm\theta} + \Gamma^m_0 \tan \phi_0 \cos \phi_2 e^{-jm(\theta+\pi)} \right] \quad (64g)$$

$$I_2^m(\phi_2) = jB_1 \left[ -Y(\theta) \cos \phi_2 e^{-jm\theta} - Y(\theta + \pi) \Gamma^m_0 \tan \phi_0 \sin \phi_2 e^{-jm(\theta+\pi)} \right] \quad (64h)$$

$$2. \quad \beta = 0 \text{ or } \cot^2 \phi_0 = \frac{Y(\theta)}{Y(\theta + \pi)} \quad (65a)$$

$$B_1 = B_4 = B_5 = B_8 = 0 \quad (65b)$$

$$B_3 = -B_7 = \Gamma^{m_0} \cot \phi_0 B_2 \quad (65c)$$

$$B_6 = B_2 \quad (65d)$$

$$V_1^m(\phi_1) = B_2 \left[ \cos \phi_1 e^{-jm\theta} + \Gamma^{m_0} \cot \phi_0 \sin \phi_1 e^{-jm(\theta+\pi)} \right] \quad (65e)$$

$$I_1^m(\phi_1) = jB_2 \left[ -Y(\theta) \sin \phi_1 e^{-jm\theta} + Y(\theta + \pi) \Gamma^{m_0} \cot \phi_0 \cos \phi_1 e^{-jm(\theta+\pi)} \right] \quad (65f)$$

$$V_2^m(\phi_2) = B_2 \left[ \cos \phi_2 e^{-jm\theta} - \Gamma^{m_0} \cot \phi_0 \sin \phi_2 e^{-jm(\theta+\pi)} \right] \quad (65g)$$

$$I_2^m(\phi_2) = jB_2 \left[ -Y(\theta) \sin \phi_2 e^{-jm\theta} - Y(\theta + \pi) \Gamma^{m_0} \cot \phi_0 \cos \phi_2 e^{-jm(\theta+\pi)} \right] \quad (65h)$$

The first passband of the vane-loaded ladder is shown in Fig. 9. It is identical to that of the interdigital line except for the ladder resonance at midband.

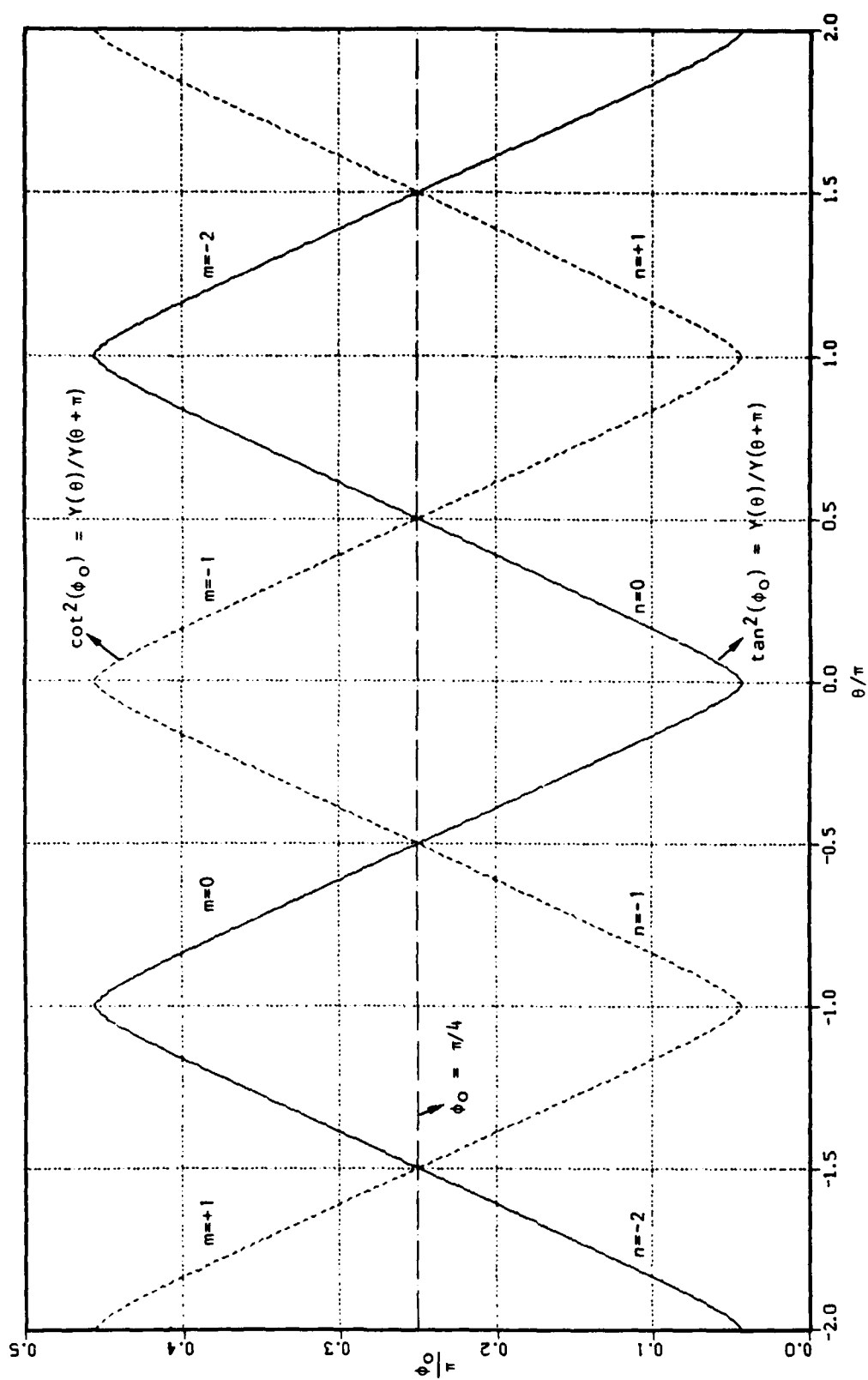


Fig. 9. First passband of the vane-loaded ladder slow-wave circuit.

### C. Beam Coupling Impedance

The beam coupling impedance is repeated here as Eq. 66 for convenience.

$$K_n(\theta) = \frac{1}{2\phi_b} \int_{-\phi_b}^{+\phi_b} K_n(\theta, \phi) d\phi \quad (66)$$

In this expression,

$$K_n(\theta, \phi) = \frac{1}{2} \frac{E_n E_n^*}{\beta_n^2 v_g W_s} \quad (67)$$

and all other quantities are defined as before. It is again assumed that the beam just grazes the circuit at the interface between Regions 1 and 2 (see Fig. 6(b)). Like the dispersion characteristic determined in Section B, the coupling impedance is derived here exactly as it is done in Chapter II. Some very minor differences arise because of the altered electric field distribution.

#### 1. Group Velocity $v_g$

Because the dispersion characteristic for the propagating mode is unchanged from Chapter II, the group velocity is also unchanged. It is given by

$$v_g = \frac{d\omega}{d\beta} \frac{d\beta}{d\theta} = \ell \frac{d\beta}{d\theta} = \frac{\ell c}{2h} H(\theta) \quad (68)$$

where  $H(\theta)$  is given by Eq. 31.

## 2. Stored Energy Per Pitch

The total stored energy per pitch,  $W_s$ , for the vane-loaded ladder is the sum of the stored energies in each region. A comparison of Eqs. 64 and 22 shows the voltage distributions in each region are identical to that of the interdigital line, with the inconsequential exception that the  $\sin \phi$  component of  $V_2$  is negated, as it must be for continuity across the centerline. Since  $W_s$  is derived from the voltage, this indicates that the stored energy in either region is the same as for the interdigital line. Thus, the total stored energy per pitch for the vane-loaded ladder is exactly twice the value given by Eq. 37, or

$$W_s = \frac{2h}{1c} Y(\theta) B_1^2 \quad (69)$$

## 3. Electric Field Distribution $E_n E_n^*$

Like  $W_s$ , the z-directed electric field,  $E_n$ , is derived from the voltage. Therefore, the electric field distributions,  $E_n E_n^*$ , in each region are the same as for the interdigital line. For the space harmonics of interest, they are

$$\left( E_o E_o^* \right)_{I,II} = \frac{4B_1^2}{l^2} \sin^2 \frac{\theta}{2} \frac{\sin^2 \left[ \frac{\theta q}{2l} \right]}{\left[ \frac{\theta q}{2l} \right]^2} \sin^2 \phi_{I,II} \quad (70)$$

$$\left( E_{+1} E_{+1}^* \right)_{I,II} = \frac{4B_1^2}{l^2} \tan^2 \phi_o \cos^2 \frac{\theta}{2} \frac{\sin^2 \left[ \frac{(\theta + \pi)q}{2l} \right]}{\left[ \frac{(\theta + \pi)q}{2l} \right]^2} \cos^2 \phi_{I,II} \quad (71)$$

$$\left(E_{-1}E_{-1}^*\right)_{I,II} = \frac{4B_1^2}{\ell^2} \tan^2 \phi_0 \cos^2\left(\frac{\theta}{2}\right) \frac{\sin^2 \left[ \frac{(\pi - \theta)q}{2\ell} \right]}{\left[ \frac{(\pi - \theta)q}{2\ell} \right]^2} \cos^2 \phi_{I,II} \quad (72)$$

$$\left(E_{-2}E_{-2}^*\right)_{I,II} = \frac{4B_1^2}{\ell^2} \sin^2 \frac{\theta}{2} \frac{\sin^2 \left[ \frac{(2\pi - \theta)q}{2\ell} \right]}{\left[ \frac{(2\pi - \theta)q}{2\ell} \right]^2} \sin^2 \phi_{I,II} \quad (73)$$

Those distributions which were formerly edge modes now reach a local maximum at the center of the circuit (i.e., the true centerline where  $\phi_1 = +\phi_0$  and  $\phi_2 = -\phi_0$ ). Those which were formerly center modes now reach a local minimum there.

#### 4. Final Expressions for Beam Coupling Impedance

The final expressions for  $K(\theta)$  are obtained as before by substituting the expressions for  $v_g$ ,  $W_s$ , and  $E_n E_n^*$  into Eq. 66 and then integrating over the beamwidth. The electric field distributions for all harmonics are symmetrical about the centerline, and therefore it is necessary to integrate only over that portion of the beam which is in Region I. Integrating over the entire beam width would not change the result because the average electric field acting on the electrons would not change. The final expressions are

$$K_i(\theta) = K_i^1 * K_i^2 \quad i = 0, +1, -1, -2 \quad (74)$$

where

$$\begin{aligned}
 K_{0,+1}^1 &= K_{-2,-1}^1 = \frac{1}{\phi_b} \int_{\phi_0 - \phi_b}^{\phi_0} \frac{\sin^2 \phi}{\cos^2 \phi} \delta \phi \\
 &= \frac{1}{2} \pm \frac{\sin(2\phi_b)}{4\phi_b} \pm \frac{\sin[2(\phi_0 - \phi_b)]}{4\phi_b}
 \end{aligned} \tag{75}$$

$$K_0^2 = \frac{4}{\theta^2 H(\theta) Y(\theta)} \sin^2\left(\frac{\theta}{2}\right) \frac{\sin^2\left[\frac{\theta q}{2l}\right]}{\left[\frac{\theta q}{2l}\right]^2} \tag{76a}$$

$$K_{+1}^2 = \frac{4}{(\theta + \pi)^2 H(\theta) Y(\theta)} \tan^2 \phi_0 \cos^2\left(\frac{\theta}{2}\right) \frac{\sin^2\left[\frac{(\theta + \pi)q}{2l}\right]}{\left[\frac{(\theta + \pi)q}{2l}\right]^2} \tag{76b}$$

$$K_{-1}^2 = \frac{4}{(\pi - \theta)^2 H(\theta) Y(\theta)} \tan^2 \phi_0 \cos^2\left(\frac{\theta}{2}\right) \frac{\sin^2\left[\frac{(\pi - \theta)q}{2l}\right]}{\left[\frac{(\pi - \theta)q}{2l}\right]^2} \tag{76c}$$

$$K_{-2}^2 = \frac{4}{(2\pi - \theta)^2 H(\theta) Y(\theta)} \sin^2\left(\frac{\theta}{2}\right) \frac{\sin^2\left[\frac{(2\pi - \theta)q}{2l}\right]}{\left[\frac{(2\pi - \theta)q}{2l}\right]^2} \tag{76d}$$

The values given here for  $K^2$  are identical to those given in Chapter II, except for the factor of two decrease due to the factor of two increase in  $w_s$ . These expressions are plotted in Figs. 10 and 11 for various beamwidths.

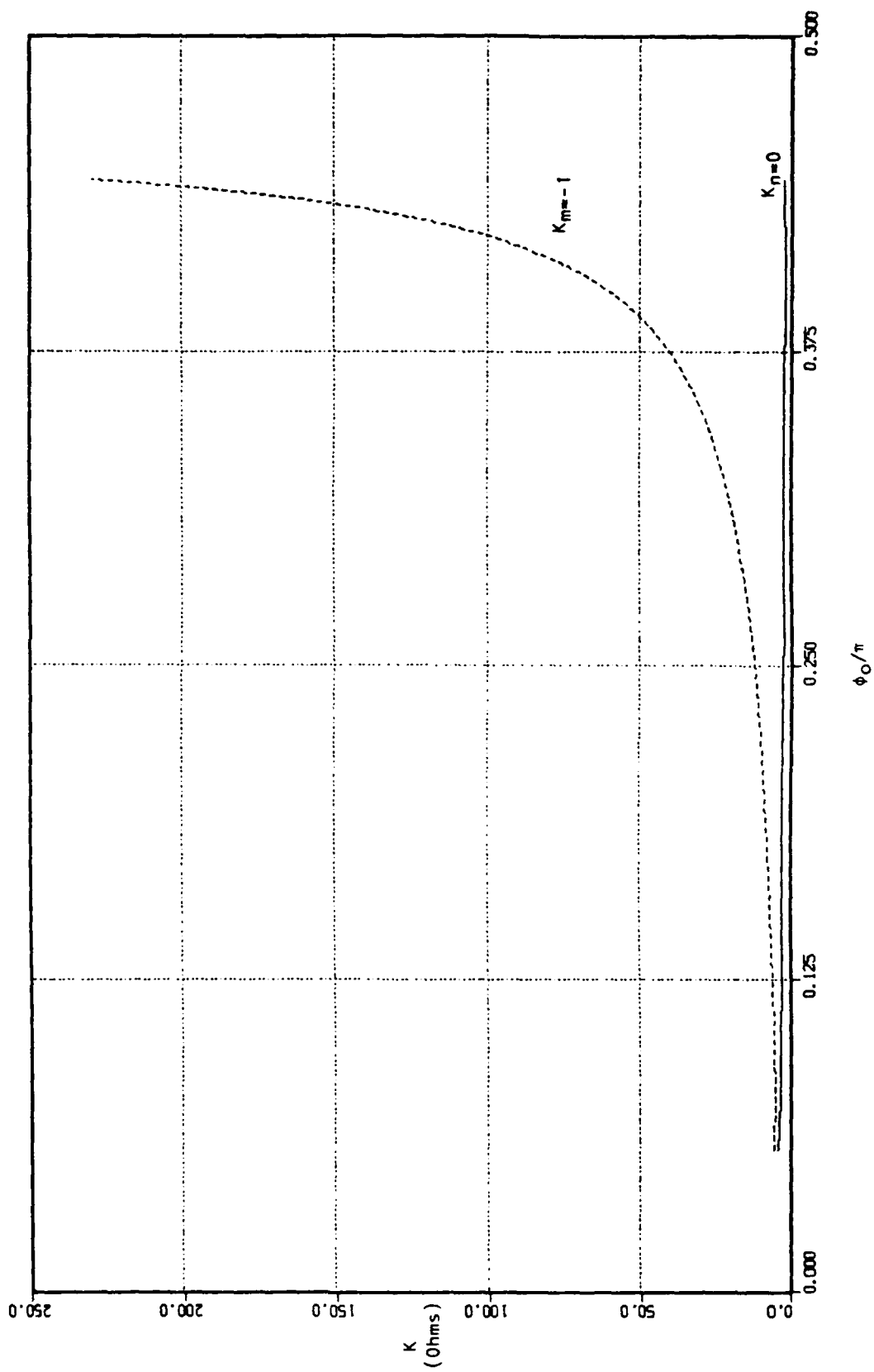


Fig. 10a. Beam coupling impedance for the primary vane-loaded ladder space harmonics ( $\phi_b = \phi_0, 2\phi_0$ ).



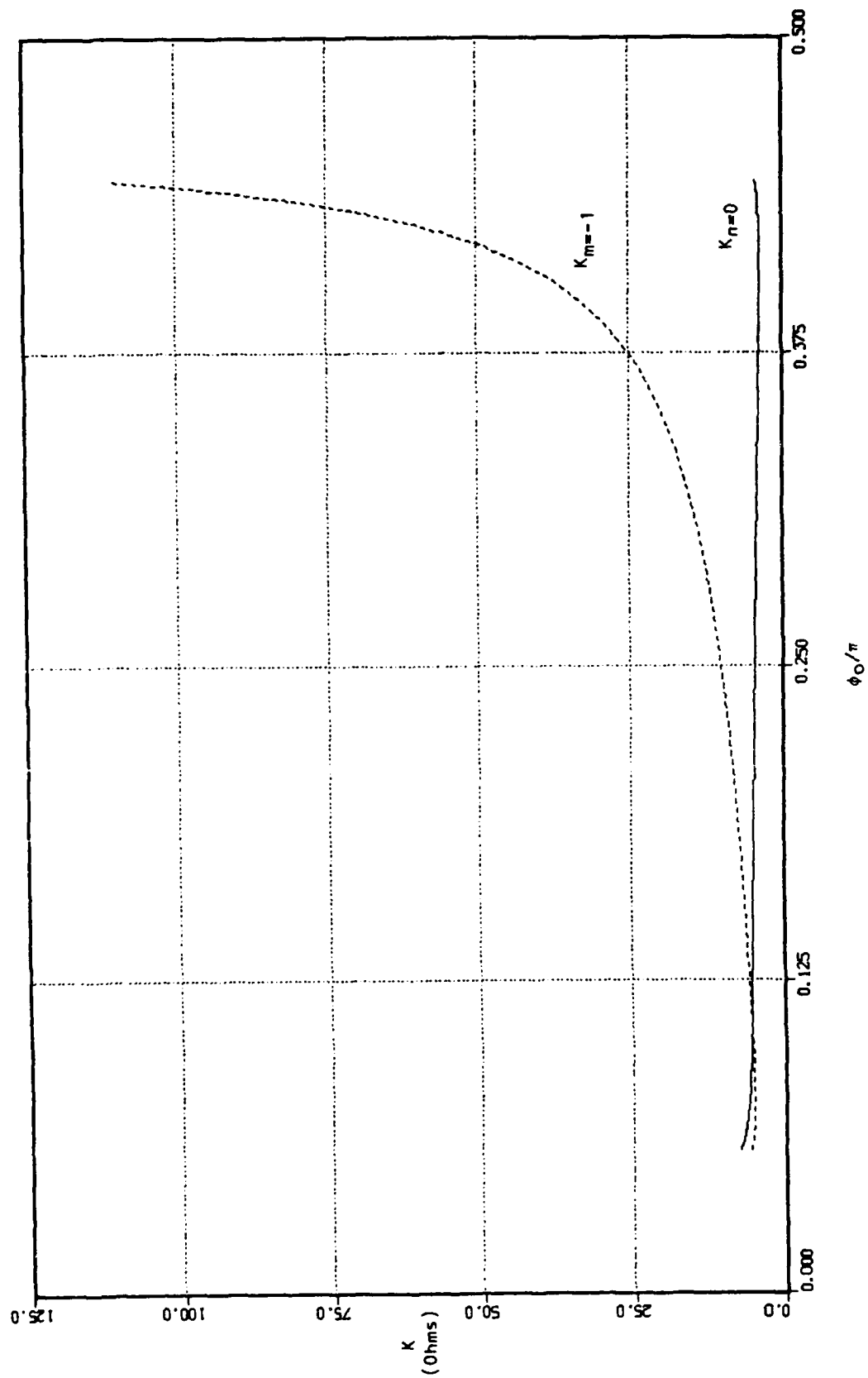


Fig. 10b. Beam coupling impedance for the primary vane-loaded ladder space harmonics ( $\phi_b = \phi_0/2$ ).

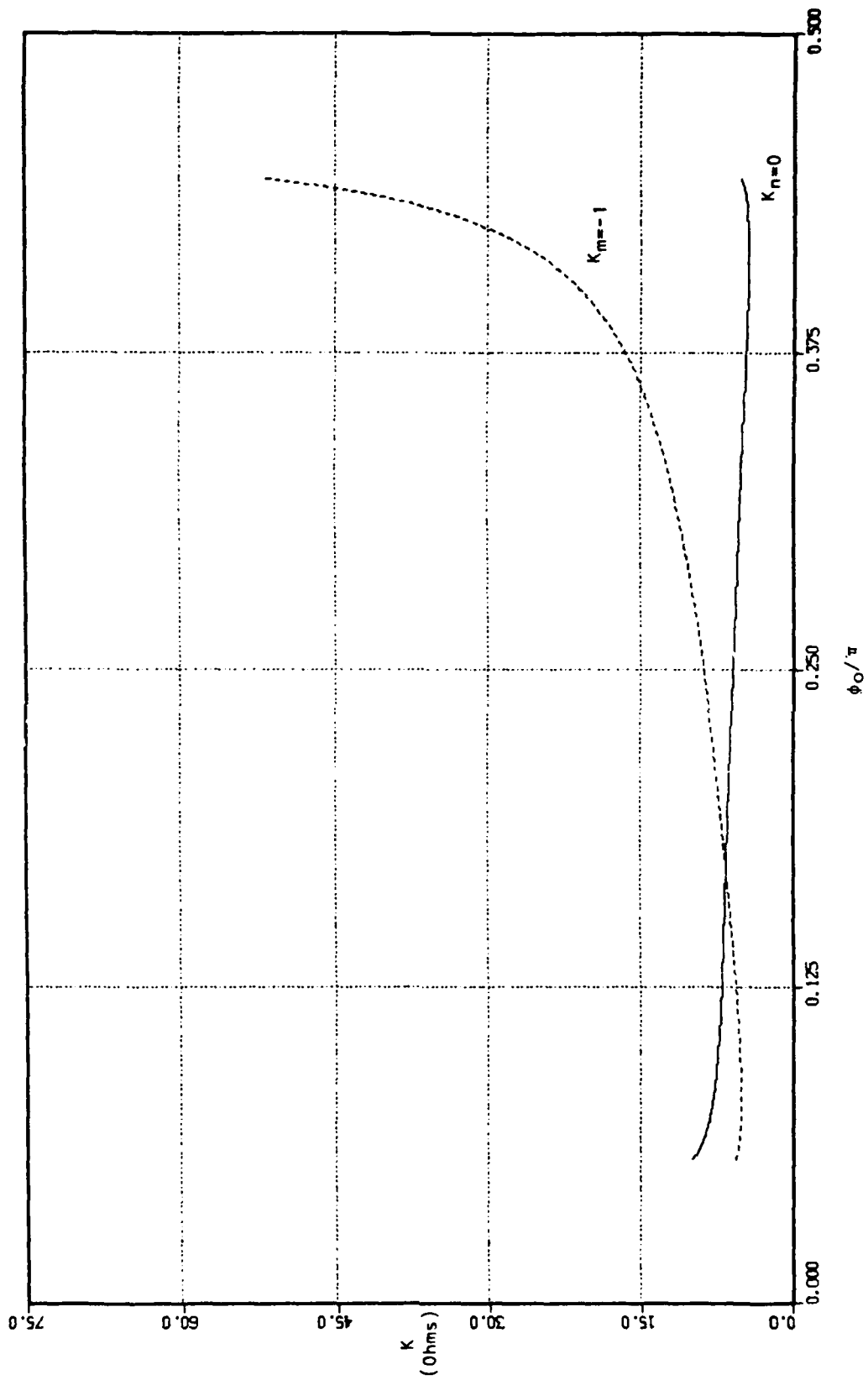


Fig. 10c. Beam coupling impedance for the primary vane-loaded ladder space harmonics ( $\phi_b = \phi_0/4$ ).

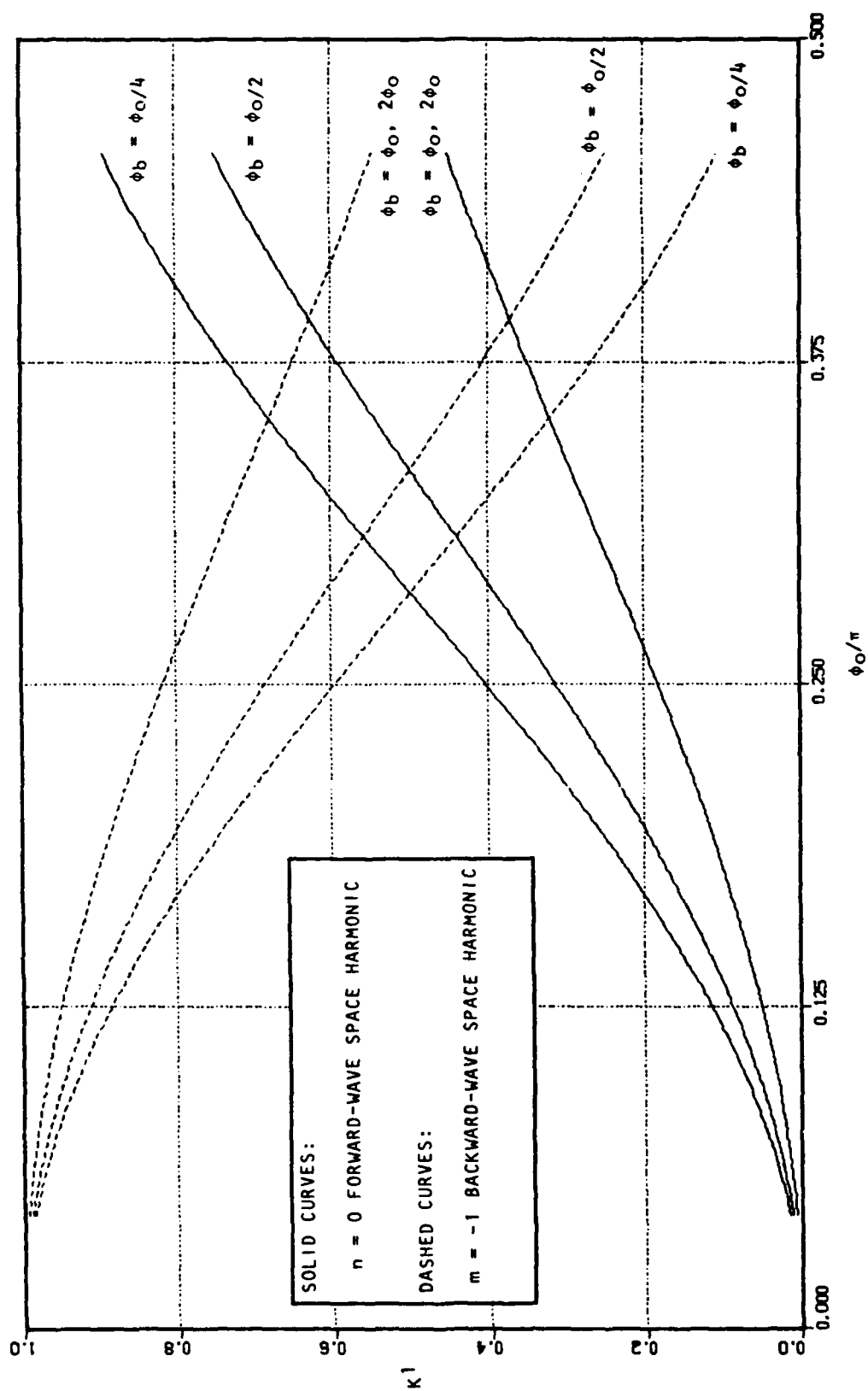


Fig. 10d.  $K^1$  for the primary vane-loaded ladder space harmonics ( $\phi_b = 2\phi_o, \phi_o, \phi_o/2, \phi_o/4$ ).

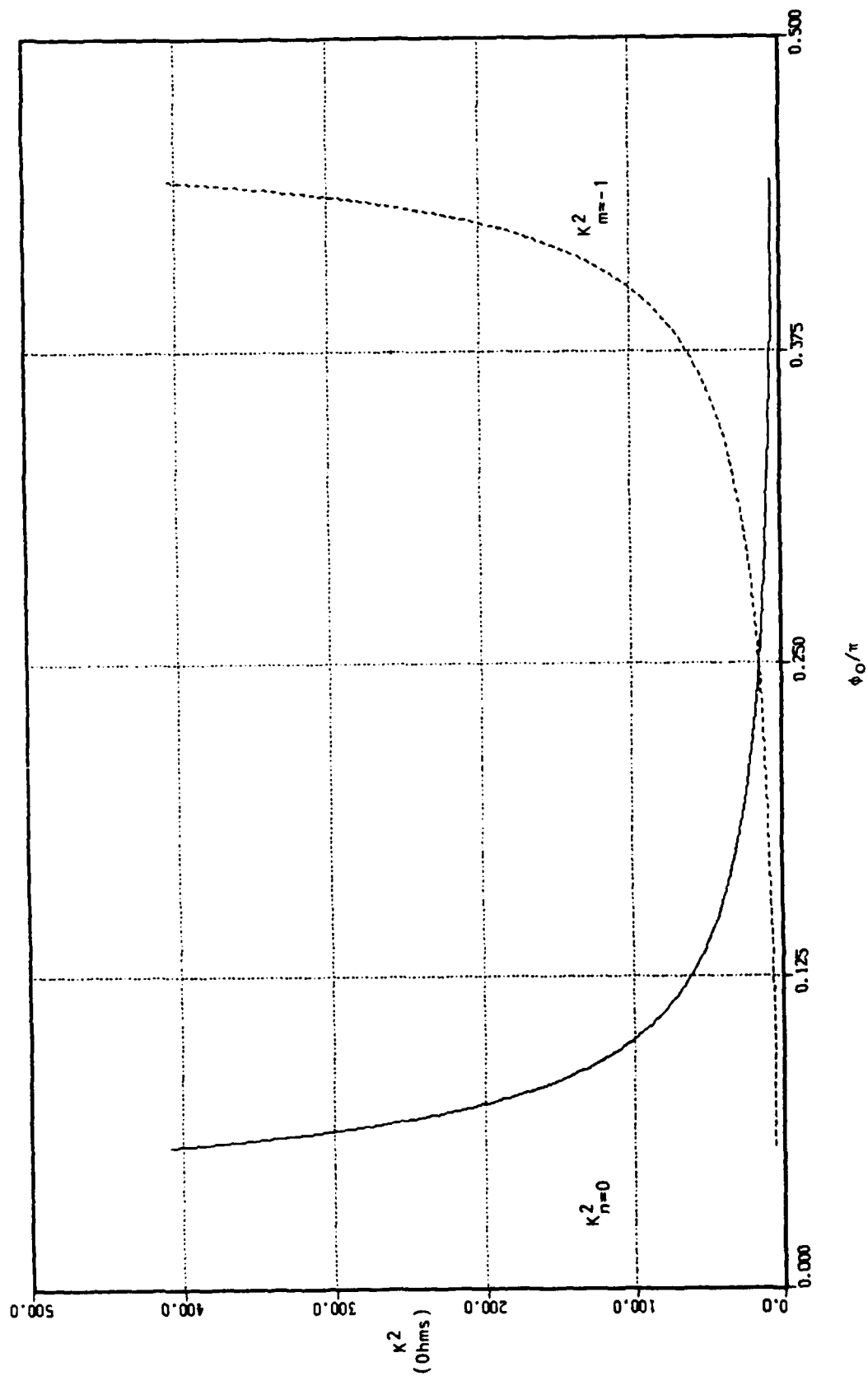


Fig. 10e.  $K^2$  for the primary vane-loaded ladder space harmonics.

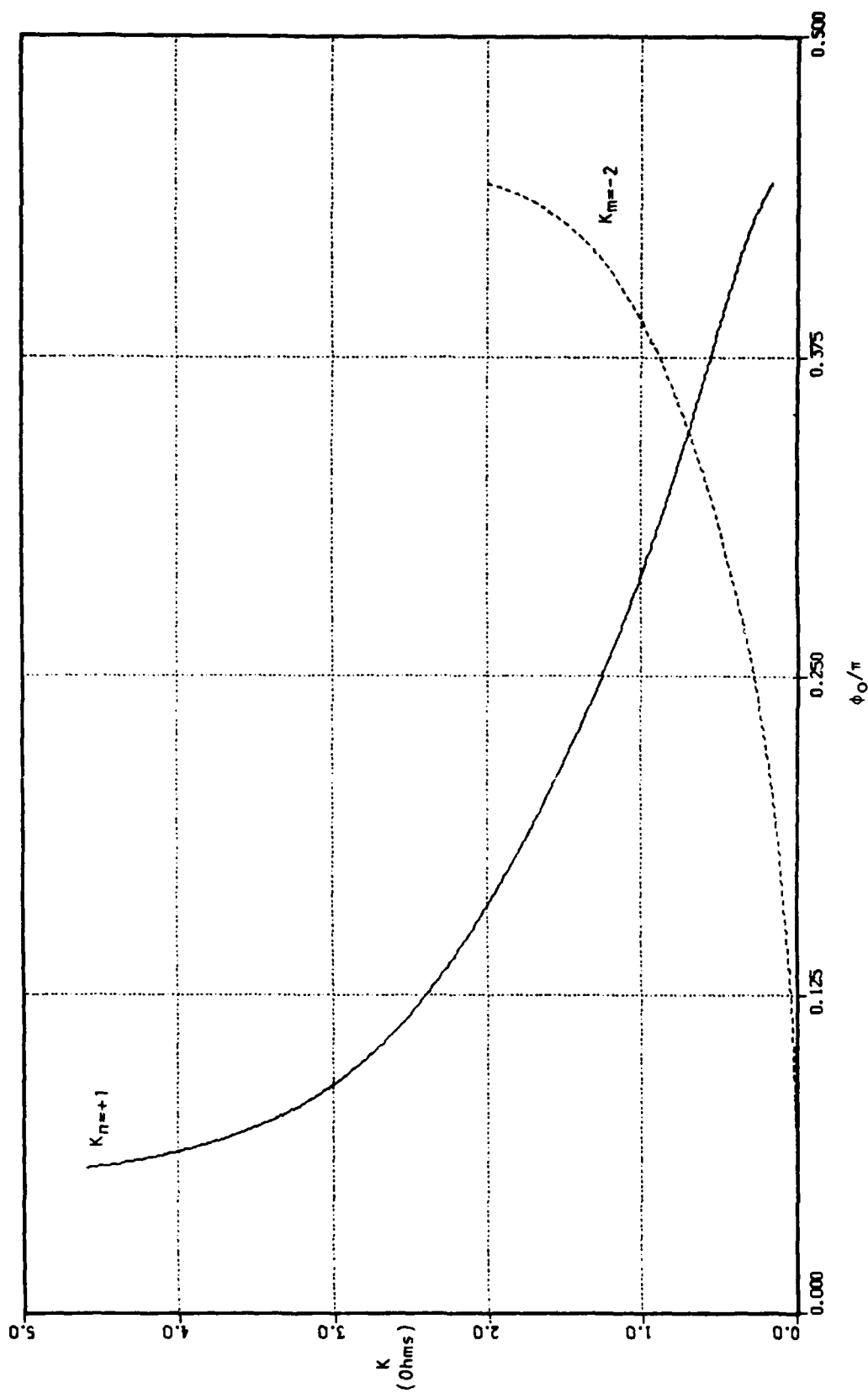


Fig. 11a. Beam coupling impedance for the secondary vane-loaded ladder space harmonics ( $\phi_b = \phi_0, 2\phi_0$ ).

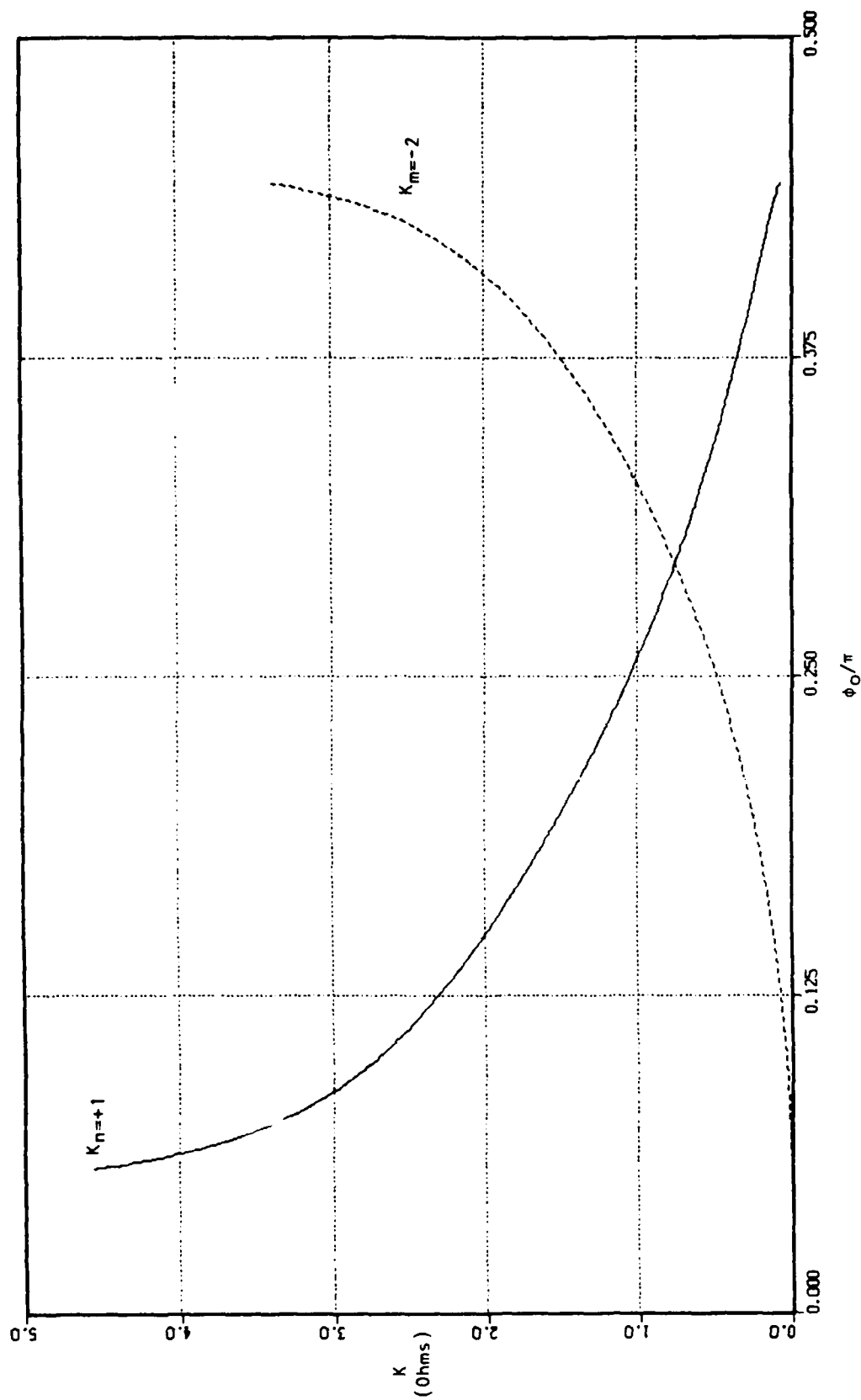


Fig. 11b. Beam coupling impedance for the secondary vane-loaded ladder space harmonics ( $\phi_b = \phi_0/2$ ).

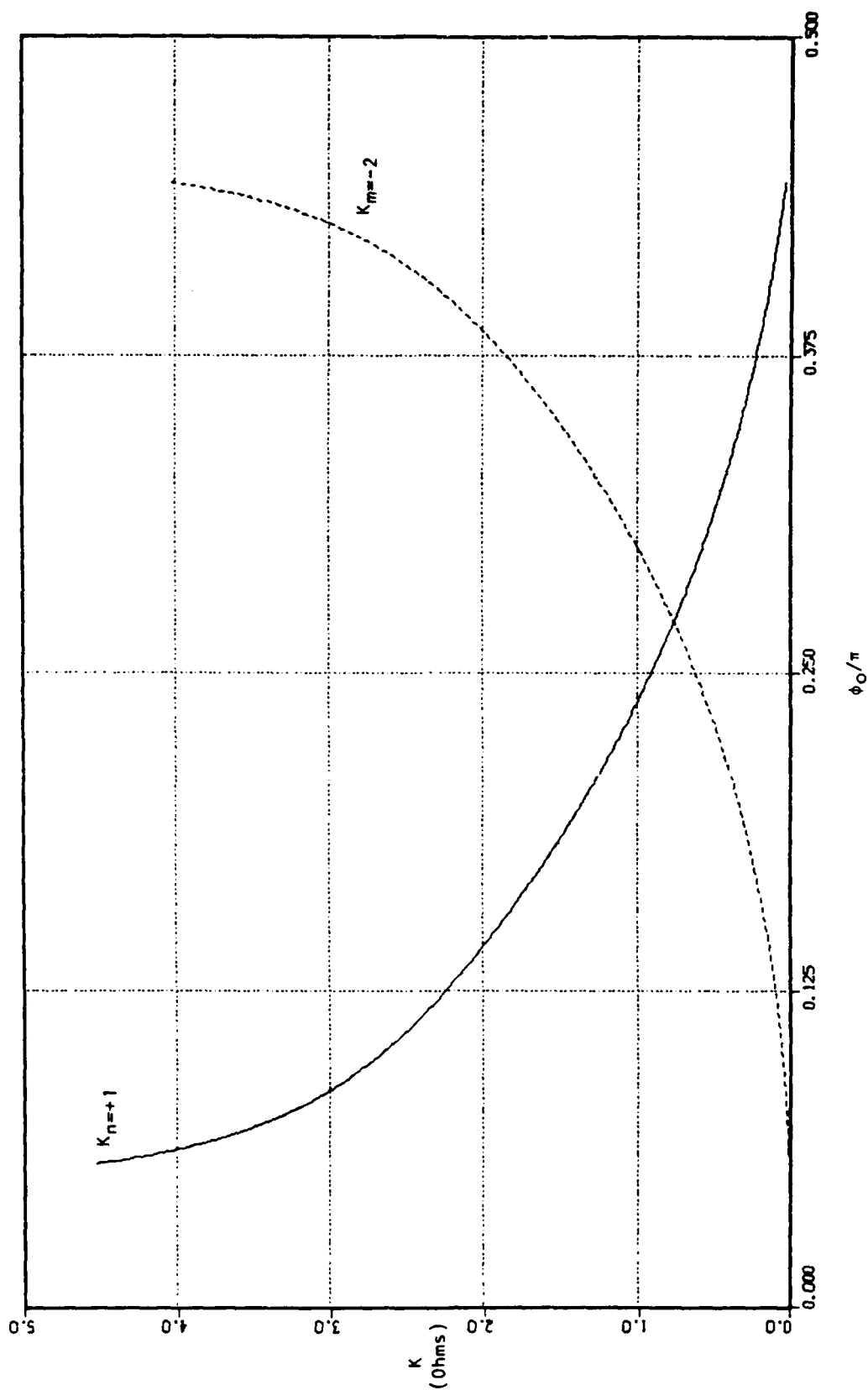


Fig. 11c. Beam coupling impedance for the secondary vane-loaded ladder space harmonics ( $\phi_b = \phi_0/4$ ).

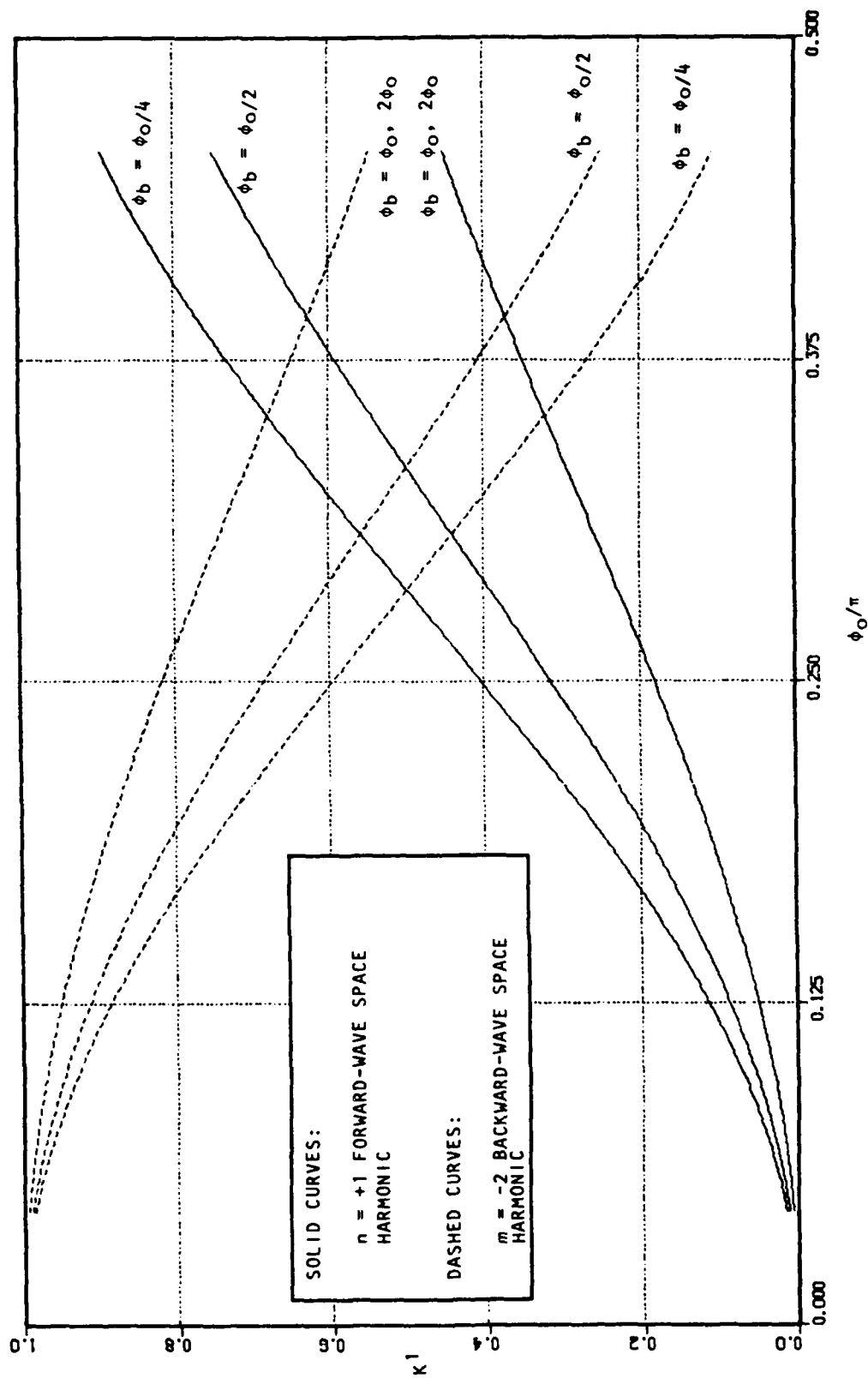


Fig. 11d.  $K^1$  for the secondary vane-loaded ladder space harmonics ( $\phi_b = 2\phi_0, \phi_0, \phi_0/2, \phi_0/4$ ).



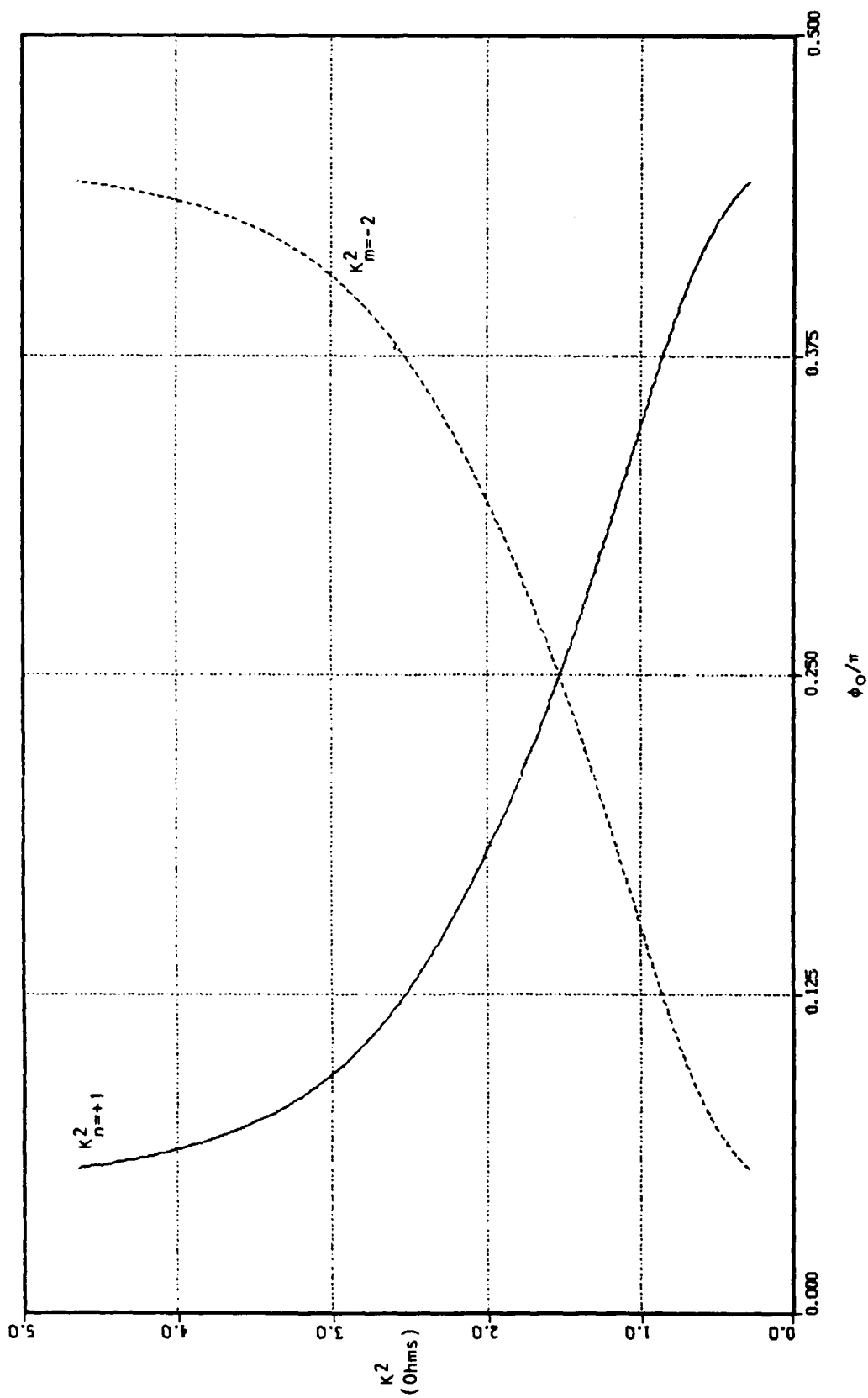


Fig. 11e.  $K^2$  for the secondary vane-loaded ladder space harmonics.

#### IV. DISCUSSION

For completeness, Fletcher's key observations<sup>1</sup> on the interdigital line dispersion will be included here. As mentioned, Eqs. 22 and 23 actually describe the space harmonic structure of a single circuit mode. This is more apparent after an examination of the properties of  $Y(\theta)$ , namely,

$$Y(\theta) = Y(-\theta) = Y(\theta + n2\pi), \quad n = \text{any integer} \quad (77a)$$

$$Y(\theta + \pi) = Y(\theta - \pi) = Y(\pi - \theta) \quad (77b)$$

Because  $Y(\theta + 2\pi) = Y(\theta)$ , Eqs. 22 at  $\theta = \theta_0 + \pi$  are identical to Eqs. 23 at  $\theta = \theta_0$ , except for the trivial nomenclature changes  $A_1 \rightarrow A_3$  and  $A_2 \rightarrow A_4$ . The two sets of equations merely describe different subsets of the space harmonics. It also follows from Eq. 77b that  $(\theta, \phi_0) = (\pi/2, \pi/4)$  is the central point in the dispersion of any interdigital line, regardless of the exact dimensions, since

$$\left. \frac{Y(\theta)}{Y(\theta + \pi)} \right|_{\theta=\pi/2} = \left. \frac{Y(\theta)}{Y(\pi - \theta)} \right|_{\theta=\pi/2} = 1 = \tan^2 \phi_0 \quad (78)$$

which in turn implies

$$\phi_0 = \frac{\pi}{4} \quad (79)$$

in the first passband.

The bandwidth for a given space harmonic is defined as the frequency range over which the phase velocity,  $v_p$ , for that component does not vary by more than  $\pm 1$  percent from its midband value,  $v_0$ . Fletcher<sup>1</sup> claimed that bandwidths of up to  $\pm 16$  percent can be obtained for the primary space harmonics with optimum finger separation and thickness and has provided guidelines for optimizing an interdigital line of a given pitch. However, computer simulations prove his guidelines to be in error. This is most likely due to the use of an incorrect admittance function. Several trials with the same computer simulation led to the dimensions given in parentheses in Fig. 1 (a rigorous re-examination of the optimizing guidelines was not undertaken here). The phase velocities for the components of interest are plotted in Fig. 12. Using the given definition, the bandwidth for the fundamental forward-wave space harmonic is approximately  $\pm 8$  percent at a center frequency of 5.36 GHz. In a microwave amplifier, this would be instantaneous bandwidth. In comparison, the bandwidth for the  $n = +1$  forward-wave harmonic is  $\pm 2$  percent at the same center frequency. It is possible to improve the bandwidth of this component, but that of the fundamental can always be made greater. Therefore, forward-wave interaction with the fundamental space harmonic would be preferable.

The beam coupling impedances show why the interdigital line enjoys considerable popularity as a backward-wave circuit and virtually none as a forward-wave circuit. Consider first the primary space harmonics. Figure 4(c) is a plot of  $K_0^2$  and  $K_{-1}^2$ . It can be seen that these factors have a sort of antisymmetry about the center of the band. Initially, one would expect this behavior to prevail. However,  $K_0^1$  offsets  $K_0^2$  in

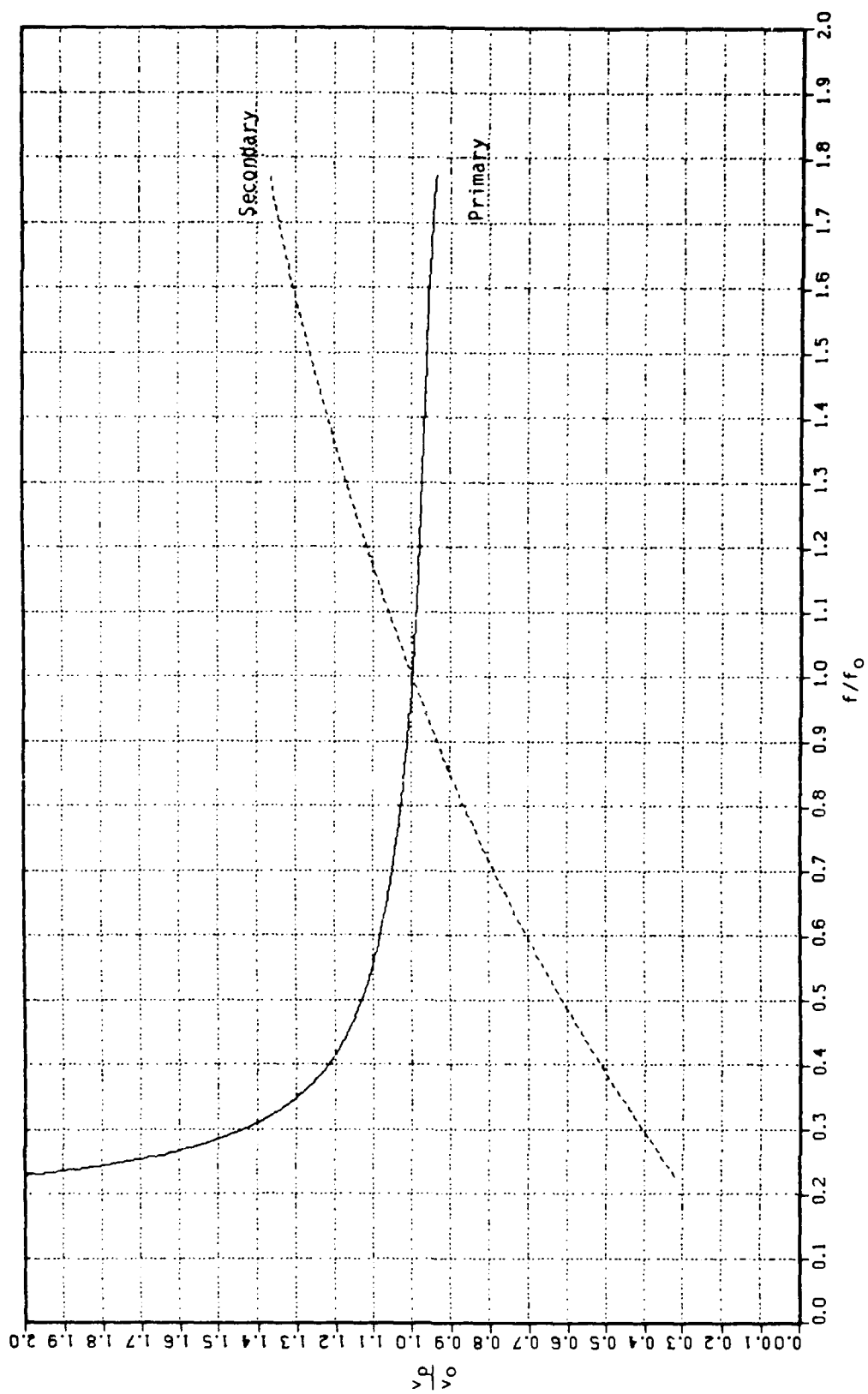


Fig. 12. Phase velocities for the primary and secondary forward-wave components (both circuits).

the final expression. A plot of  $K_0^1$  and  $K_{-1}^1$  is shown in Fig. 4(b). This reveals what is intuitively obvious from the electric field distributions. The fundamental forward-wave harmonic is an edge mode, which implies it has a null at the center of the circuit. Integrating across this null produces a small value for  $K_0^1$ , particularly at the low end of the band where  $\phi_0$  is small. Conversely, the backward-wave component is a center mode. It reaches a maximum at the center of the circuit. Integrating across this maximum gives a much larger value for  $K_{-1}^1$ . Only at the high end of the band, as  $\phi_0$  approaches  $\pi/2$ , do the two factors approach equality. In the final expressions, which are plotted in Fig. 4(a), these factors combine to make  $K_{-1}$  significantly greater than  $K_0$  over most of the band. This figure also shows  $(K_{-1}/K_0)_{\phi_0=\pi/4} = 4.5$ . As a result, it would be difficult to prevent midband oscillations if the fundamental forward-wave space harmonic were utilized in a microwave amplifier.

An alternative would be to use the  $n = +1$  forward-wave harmonic. In this domain, the factors  $K^2$  exhibit the same relative behavior as in the primary domain. This is shown in Fig. 5(c). However, the functional dependencies of the electric field distributions are reversed from those discussed above. The forward-wave harmonic is a center mode, and the backward-wave harmonic is an edge mode. As a result, the relative behavior of  $K^1$  is reversed, as is shown in Fig. 5(b). The end result, shown in Fig. 5(a), is that  $K_{+1}$  is greater than  $K_{-2}$  over most, but not all, of the band. This is adequate, however, since a beam aligned with the forward-wave harmonic would only see the backward-wave harmonic at midband, where  $(K_{-2}/K_{+1})_{\phi_0=\pi/4} = 0.22$ . The price for this

improved behavior is the reduced bandwidth discussed above. Also, the impedance values are both lower than for their primary domain counterparts. This is due mainly to the larger  $\beta$  for these components.

The results discussed so far suggest that the interdigital line would be a desirable amplifier circuit if it were transformed to provide better access to the fundamental forward-wave space harmonic, i.e., transformed so that the primary space harmonics possessed impedance behavior similar to that normally displayed by the components in the secondary domain. This would allow wide-band utilization of the fundamental forward-wave harmonic without the threat of oscillation. The vane-loaded ladder was designed to execute this transformation by propagating two side-by-side interdigital line modes. This preserves the wide-band dispersion while reversing (from edge to center modes and vice versa) the electric field distributions for the primary space harmonics. This in turn would affect the  $K^1$  values for these components, thereby bolstering the forward-wave coupling impedance, while decreasing that of the backward wave.

The results presented in Chapter III show that the new circuit was not entirely successful in achieving these goals. Consider first the dispersion. For the most part, the vane-loaded ladder did retain the dispersion characteristics of the interdigital line, which is not surprising since it does propagate two side-by-side interdigital line modes. In fact, because  $\alpha = 0$  for the propagating mode, both  $I_1$  and  $I_2$  go to zero where the centerline meets the rungs. This indicates that the propagating mode would be unchanged if the rungs were cut at the centerline line and a center rail were incorporated into the circuit,

i.e., if the vane-loaded ladder were constructed exactly of two adjacent interdigital lines. However, the circuit also possesses additional features which are undesirable. The first of these is the midband ladder resonance. It is unclear if the beam would strongly couple to this resonance in the presence of the propagating mode. However, Walling<sup>2</sup> has shown that the effect of the finger-end capacitances on the interdigital line is to create a small stopband at the center of the passband. If such a stopband also exists here, and it is logical to conclude that it would, the likelihood of strong coupling to this resonance is much greater. If this is so, regardless of the impedance behavior, this would essentially be a return to the case of the interdigital line, where a more strongly coupled component inhibited interaction with the fundamental forward-wave space harmonic. Furthermore, the resonance exists in all domains, so interaction with the  $n = +1$  forward-wave harmonic would be equally affected. The second feature is that the assumption of zero voltage at the center of the vanes would most likely require the link to the backwall to be shorter than that used here. This would reduce the bandwidth due to the increased back-wall loading. In short, the new circuit does not accurately preserve the interdigital line dispersion.

The circuit also fails to realize the goal of reversing the impedance behavior of the primary space harmonics through alterations of the factors  $K_{0,-1}^1$ . This is understandable after examining Figs. 13a-13c, which shows the  $\sin^2 \phi$  and  $\cos^2 \phi$  envelopes of the electric field distributions at three points across the band. This figure foreshadows the result that in altering the factor  $K^1$ , the form of the electric field

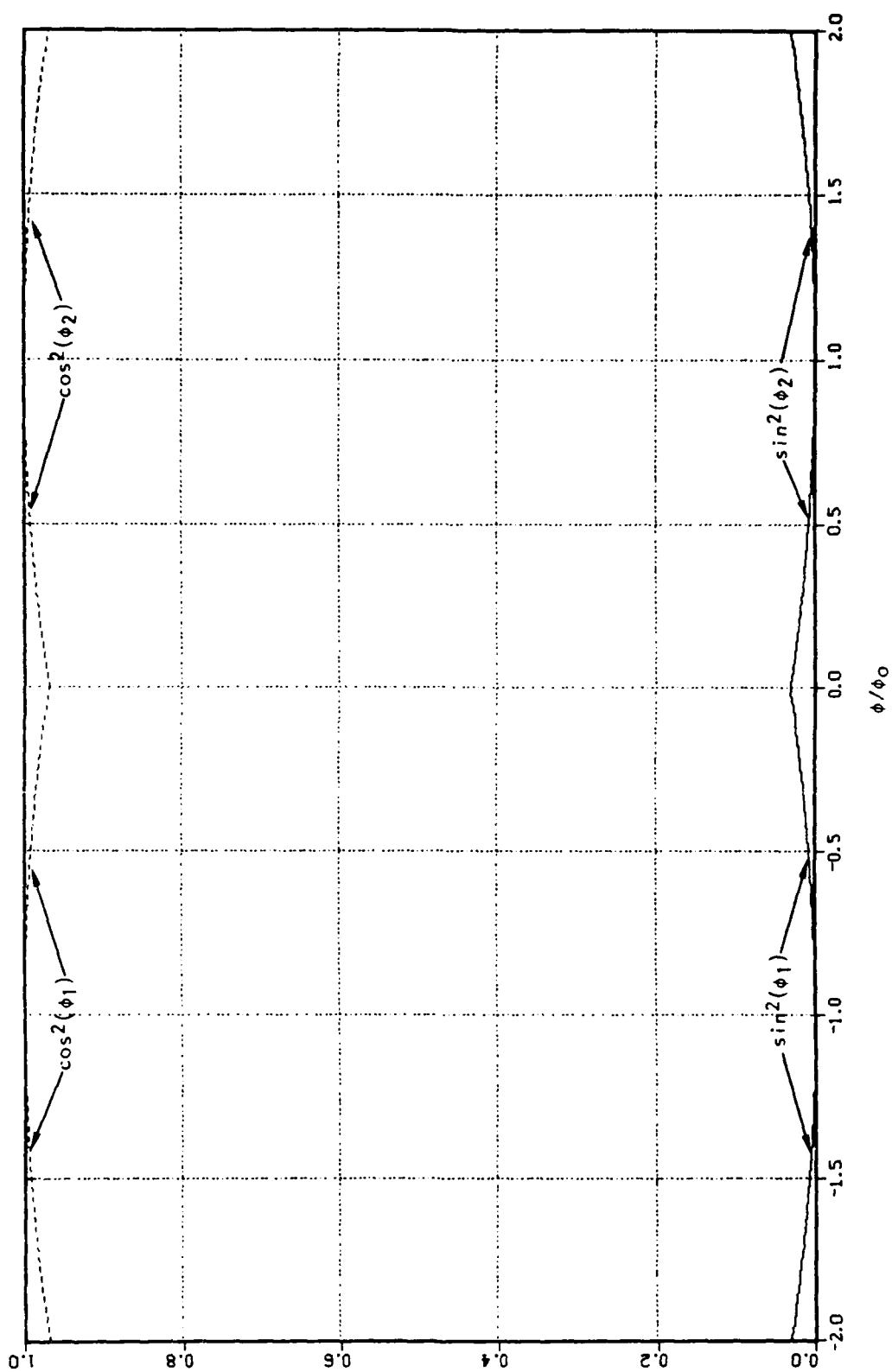


Fig. 13a. Electric field modulation for the primary vane-loaded ladder space harmonics (low end of band).



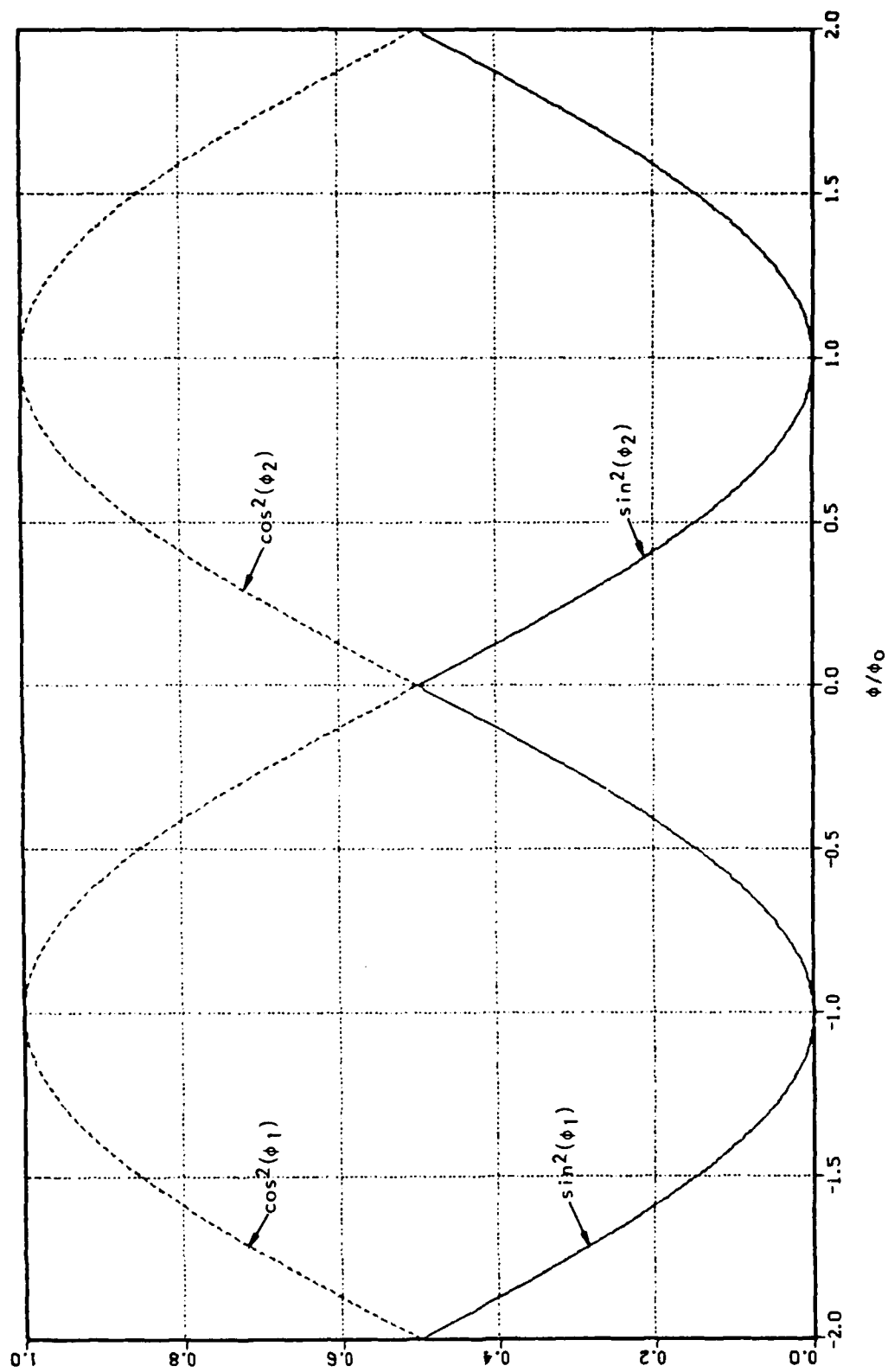


Fig. 13b. Electric field modulation for the primary vane-loaded ladder space harmonics (mid-band).

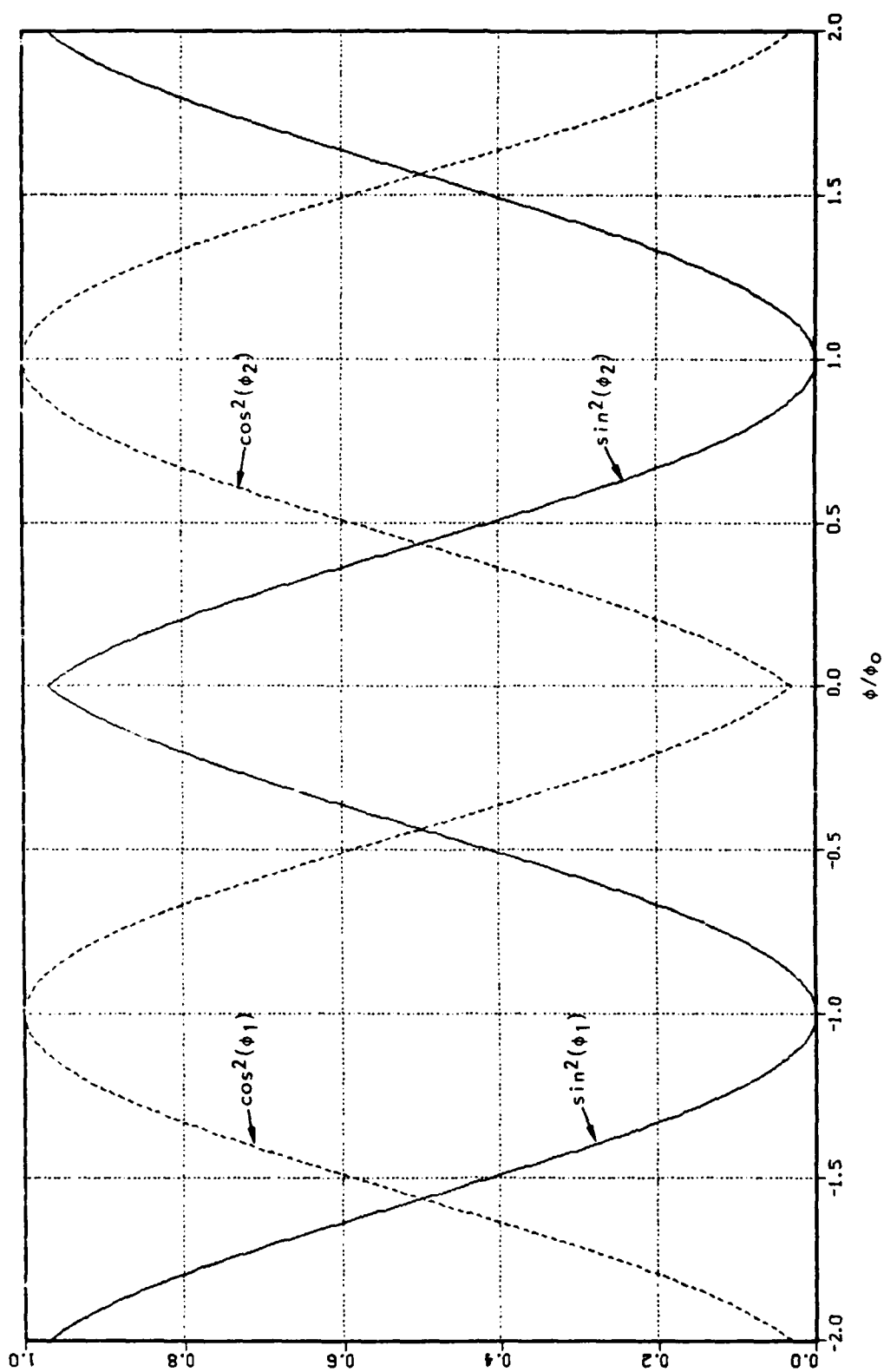


Fig. 13c. Electric field modulation for the primary vane-loaded ladder space harmonics (high end of band).

distribution will play a secondary role to the magnitudes involved. Although not a true center mode (maximum value in the center, minimum value at the edges), the modulation for the fundamental forward-wave space harmonic now reaches a local maximum at the centerline. Similarly, the  $m = -1$  backward-wave distribution now reaches a local minimum at the centerline although it is not a true edge mode. However, although somewhat displaced, the former is still essentially a  $\sin^2\phi$  distribution, and the latter is essentially a  $\cos^2\phi$  distribution. Averaging across the former produces a smaller value than for the latter. This is shown in Fig. 10(d), which shows  $K_{0,-1}^1$  for various beamwidths. For the cases  $\phi_b = 4\phi_0$  (beam spans the entire width of the circuit) and  $\phi_b = 2\phi_0$  (beam stretches from the center of Region I to the center of Region II),  $K^1$  is unchanged from its interdigital line value. This is because the electric field distributions, both here and for the interdigital line, have a half-period equal to  $\phi_0$ . Any integration over a multiple of this half-period yields the same result, indicating that the average field acting on the electrons has not changed. Only for the case  $\phi_b < \phi_0$ , and only then at the high end of the band where  $\sin \phi_0 > \cos \phi_0$ , do the new electric field distributions result in an increase in  $K_0^1$  at the expense of  $K_{-1}^1$ . Even so, this limited effect is not enough to produce the desired results. For  $\phi_b = \phi_0/4$ , the ratio  $(K_{-1}/K_0)_{\phi_0=\pi/4} = 3.13$  is still large.

The results are similar for the secondary domain, as shown in Figs. 11a-11e. As before, for  $\phi_b = 4\phi_0$  or  $\phi_b = 2\phi_0$ ,  $K^1$  is unchanged from the case of the interdigital line. However, since the electric field modulations in the domain  $1 \leq \theta/\pi \leq 2$  are the reverse of those in

the primary domain,  $\phi_b < \phi_0$  improves  $K_{-2}^1$  at the expense of  $K_{+1}^1$ . This is a step in the wrong direction. In addition, the increase stored energy on the circuit further reduces the impedance values. Thus, in this domain, the new circuit cannot improve upon the interdigital line under any circumstances.

It must be conceded that the vane-loaded ladder is not a viable candidate for use in microwave amplifiers. The results shown here indicate that an unmodified interdigital line would be a better choice when used in a backward-wave amplifier. Such an amplifier would require a voltage tuning circuit in the system, but it would possess reasonable gain and bandwidth. An even better choice, as mentioned in the introduction, is the stub-supported meander line. While by nature a narrow-band circuit, it can be ridge-loaded for improved bandwidth<sup>8</sup> when accompanied by a tuning circuit. Computer simulations of such a circuit<sup>9</sup> show its beam coupling impedance to be slightly higher (for the most part) than that for the interdigital line. Furthermore, it offers the simple advantage that cooling fluids can be run directly through the circuit, giving it a greater power-handling capability. These latter two factors permit the circuit to be used in distributed emission devices as well as in injected beam devices. Like the stub-supported meander line, most typical crossed-field amplifier (CFA) slow-wave circuits enjoy these advantages and would therefore be preferred over both the interdigital line and its derivative, the vane-loaded ladder.

## V. CONCLUSION

This thesis has investigated the dispersion and beam coupling impedance of the vane-loaded ladder slow-wave circuit. The vane-loaded ladder is a circuit conceived as a consolidation of two side-by-side interdigital lines. This configuration was designed to preserve the dispersion characteristics of the interdigital line, while improving the accessibility of the fundamental forward-wave space harmonic. Such a circuit would serve as a wide-band alternative to the typically narrow-band slow-wave circuits, such as the stub-supported meander line, which are currently employed in crossed-field amplifiers (CFA's).

The results showed that the vane-loaded ladder was not successful in achieving the desired goals. From the standpoint of dispersion, its propagating mode is identical to that of the interdigital line. However, it also possesses the additional obstacle of a midband ladder resonance, which, it is believed, would be strongly coupled to a beam aligned with the fundamental forward-wave space harmonic. Furthermore, it is anticipated that the nature of the circuit would require significant backwall loading, which in turn would further reduce the bandwidth.

It was also discovered that the impedance behavior of the circuit was not significantly different from that of the interdigital line. In the primary domain, the backward-wave component still dominates and therefore carries the threat of unwanted oscillations. Only under limited circumstances do the altered electric field distributions of the new circuit help to alleviate this problem; even so, the changes induced are not significant. Similar results hold true for the secondary

domain. Overall, it is conceded that typical CFA circuits, such as the stub-supported meander line, enjoy several advantages over the vane-loaded ladder and the interdigital line from which it was derived.

## REFERENCES

1. R. C. Fletcher, "A Broad-Band Interdigital Circuit for Use in Traveling-Wave-Type Amplifiers," Proceedings of the IRE, Vol. 40, August 1952, pp. 951-958.
2. J. C. Walling, "Interdigital and Other Slow Wave Structures," Journal of Electronics and Control, Vol. 3, March 1957, pp. 239-258.
3. E. A. Ash and A. C. Studd, "A Ladder Structure for Millimeter Waves," IRE Transactions on Electron Devices, July 1961, pp. 294-302.
4. J. R. Pierce, Traveling Wave Tubes, D. Van Nostrand Company, New York, 1950.
5. J. Arnaud, "Circuits for Traveling Wave Crossed-Field Tubes," in Crossed-Field Microwave Devices, Vol. 1, E. Okress, Ed., Academic Press, Inc., New York, 1961.
6. J. R. Pierce, "Propagation in Linear Arrays of Parallel Wires," IRE Transactions on Electron Devices, Vol. ED-2, January 1955, pp. 13-24.
7. S. P. Yu and P. N. Hess, "Slow-Wave Structures for M-Type Devices," IRE Transactions on Electron Devices, January 1962, pp. 51-57.
8. J. Froom, A. Pearson, E. A. Ash, and A. W. Horsley, "Ridge-Loaded Ladder Lines," IEEE Transactions on Electron Devices, Vol. ED-12, No. 7, July 1965, pp. 411-421.
9. N. Dionne, Raytheon Company, private communications.

# APPENDIX A

## LIST OF SYMBOLS

$A_1-A_4$	Voltage coefficients for interdigital line
$B_1-B_8$	Voltage coefficients for vane-loaded ladder
$b$	Half-width of strip beam
$c$	Free-space speed of light
$d$	Thickness of circuit elements
$E_n$	Z-directed electric field for nth space harmonic
$h$	Half (quarter)-length of interdigital (vane-loaded ladder) elements
$I$	Circuit current
$J$	$\sqrt{-1}$
$K$	Beam coupling impedance
$K^1$	Beam integration factor
$K^2$	Composite of other impedance factors
$\lambda$	Pitch of circuit
$L$	Period of circuit
$m_0$	Index for circuit elements
$m$	Index for backward-wave space harmonics
$n$	Index for forward-wave space harmonics
$p$	Width of circuit elements
$P_{ta}$	Time-averaged power flow on circuit
$q$	Distance between circuit elements
$v_g$	Group velocity of all space harmonics
$v_p$	Phase velocity for a given space harmonic
$v_0$	Midband phase velocity for a given space harmonic



$V$	Circuit voltage
$\omega$	Radian frequency
$w_b$	Distance to backwall
$w_s$	Distance to sole
$W_s$	Stored energy per pitch
$Y$	Admittance of circuit
$Y_o$	Admittance of free space
$\alpha$	$q/p$
$\alpha=0,$ $\beta=0$	Propagating modes
$\beta_n$	Propagation constant for nth space harmonic
$\theta$	Phase shift per pitch
$\phi$	Normalized distance
$\phi_o$	Normalized $h$
$\Gamma$	$(-1)$